

## TURBINE BLADE COOLING BY AIR USING DIFFERENT METHODS

Arkan K. Al-Taie  
Dept. Mechanical Eng.  
Univ. Technology

Najlaa A. Hussain  
Dept. Mechanical Eng.  
Univ. Babylon

### ABSTRACT

The determination of temperature distribution within a turbine blade is important in regards to avoid excessive high metal temperatures and temperature gradients. The prediction of temperature distribution was achieved through the use of the finite difference technique, developed to solve the problem with the transformation and grid generation techniques. Steady-state two-dimensional conduction heat transfer equation was applied to the internal nodes in mesh to get the temperature distribution, where at the surface nodes (outer, inner), forced convection heat transfer equation was applied. The solution of the problem was established using computer program, which serves to solve the equations by using Gauss-Siedel iterative method. In the present study, three cases are used for thermal analyses of the blade, which requires the specification of external and internal boundary conditions. It is also found from the results obtained that the best cooling method to the turbine blade have been obtained for the third case when the blade cooled by impingement and film cooling method. It was found in the film cooled blade that the blade temperature decreases about (170 K) cooler than the blade cooled without the film cooling method. The results of thermal analyses obtained were compared with the finite element results. The comparison shows that the finite difference results give a good agreement with the finite element results with a small difference was calculated to be (3.5%) as maximum value and it fall to (0%) in most regions.

### الخلاصة

أن حساب توزيع درجة الحرارة خلال ريشة التوربين مهم لتجنب الزيادة الفائقة في درجات الحرارة والتدرج الحراري للمعدن. أن تنبؤ توزيع درجة الحرارة تحقق من خلال استخدام طريقة الفروق الحدية والتي تم تطبيقها في حل المشكلة مع أسلوب توليد الخلايا وأسلوب نقل الإحداثيات. تم تطبيق معادلة انتقال الحرارة بالتوصيل ثنائية البعد، للحالة المستقرة للعقد الداخلية في شبكة الفروق الحدية للحصول على توزيع درجات الحرارة في تلك العقد، في حين تم تطبيق معادلة انتقال الحرارة بالحمل القسري في العقد السطحية (السطح الخارجي و السطح الداخلي). تم حل المشكلة بمساعدة برنامج حاسبة والذي قام بإيجاد توزيع درجات الحرارة باستخدام طريقة (Gauss-Siedel). في هذا البحث، ثلاثة حالات دراسية تم استخدامها للتحليل الحراري للريشة والذي يتطلب وصف الشروط الحدودية الخارجية و الداخلية. وأيضاً وجدنا من النتائج التي حصلنا عليها بأن أفضل طريقة تبريد لريشة التوربين هي التي حصلنا عليها من الحالة الثالثة عندما تم تبريد الريشة باستخدام طريقة (impingement and film cooling). ولقد وجدنا بأنه في الريشة المبردة باستخدام هذه الطريقة أن درجة حرارة الريشة تقل بحوالي (170 K) عن الريشة المبردة بدون استخدام طريقة التبريد بالغشاء (film cooling method). إن النتائج التي تم الحصول عليها من التحليل الحراري قورنت مع طريقة العناصر المحددة. وقد أظهرت المقارنة تقارب كبير بين نتائج الفروقات الحدية والعناصر المحددة مع فرق قليل ممكن حسابه ليصل إلى (3.5%) كأكبر قيمة ويقل هذا الفرق ليصل إلى (0%) في معظم المناطق.

## INTRODUCTION

In order to increase the thermodynamic efficiency of a gas turbine engine, a high turbine inlet temperature is required, [1]. Therefore, the high temperature passing on the turbine blades causes thermal stress to the turbine blades materials. To reduce the effect of thermal stress upon the materials of blade, cooling of blades is required, [2]. The air cooling methods used in the turbine blade can be divided into the following categories, [3]:

1. Convection cooling.
2. Impingement cooling.
3. Film cooling.
4. Full-coverage film cooling.
5. Transpiration cooling.

The purpose of the present study is to find the temperature distribution in air-cooled turbine blades using transformed finite difference equations using body-fitted coordinate system. The work in this paper is divided into two steps, first generating a grid and secondly solving the transformed equations in the new computational coordinates.

There are numbers of numerical, experimental work and theoretical researches in this field to get the best means for improving the increase of the turbine blades operating conditions such as Walker, M.J.B., [4], 1989, introduced a master thesis that involves the determination of temperature distribution within a turbine blade for three configurations of cooled blades (circular, elliptical cooling holes, and cooling with impingement and trailing edge ejection). The determination was by the use of finite element method and for each type, the analysis was demonstrated with different specific boundary conditions and heat transfer correlations. The results are acceptable in terms of their accuracy. This was determined by applying the procedure to a test case and comparing the results with the reference results. Jaleel J.M., [5], 2001, illustrated the finite difference method with suitable approximation for curved boundary to determine the temperature distribution within air-cooled turbine blade utilizing circular cooling holes and verified the effectiveness of the irregular finite difference method on curved non-uniform shapes such as turbine blade. Kuder D.S., [6], 2003, submitted a master thesis that involves the prediction of temperature distribution in gas turbine air-cooled blades from hub to tip. It was achieved through the use of control volume technique. The control volume mesh deals with irregular boundary. Unsteady state two dimensional heat transfer was used to get the temperature distribution. The results of thermal analyses obtained in two case studies in which cooling passages were taken as (15) circular holes, with different diameters and as (3) channel passages. Her results show that the surface temperature distribution with channel cooling passages is (20%) lower than the surface temperature distribution with circular cooling passages. Marie *et al.*, [7], 2003, presented a paper to determine the flow and temperature fields around an inlet guide vane numerically by CFD method. The governing equations are solved by 3D finite-volume Navier-Stokes method. In particular the outer surface temperature, heat transfer coefficient distributions and static pressure distributions are also presented. Ken *et al.*, [8], 2000, investigated experimental tests in a low-speed wind tunnel cascade to determine the film-cooling effectiveness of the film-cooling hole geometry on turbine airfoils. The results of full coverage film-cooling and heat transfer characteristics of rotating serpentine flow passage with and without angled turbulence

promoter had been presented in the full paper. Stefan L.F., [9], 2001, have done an experimental evaluation of both standard and prototype blade designs under real base load conditions by using optical pyrometry. Pyrometry is a valuable tool for the quality assurance, since the temperature distribution of each individual blade is determined carefully. This paper describes the application of a newly developed high-resolution pyrometer to the latest prototype, the V84.3A2 60Hz 180 Mw gas turbine. Thus, using new pyrometer probes in conjunction with a continuous data acquisition mode allows reliable, highly resolved blade surface temperature measurements, where errors and potential risks for the gas turbine are minimized at the same time.

It has been shown from above researches reported here, that their mainly study concentrate on the methods to determine temperature distribution within the blade material. These methods are: analytical, experimental and numerical methods such as control volume, finite element and finite difference method. More progress is needed in present study by using finite difference method with body fitted coordinate system is made to predict the temperature distribution in turbine blade.

**PROBLEM FORMULATION**

The problem specification was taken from a well documented reference source containing the following necessary data:

1- Definition of the blade geometry shown in Figure (1), The blade incorporates an insert which serves as the jet plenum, which is perforated to form array of jet orifices, Figure (2), is giving rise to mid-chord impingement arrays which cool the pressure and suction surfaces and an initial jet orifice row at the blade leading edge. The jet orifices have a diameter ( $d$ ), a chord-wise spacing of ( $x_n$ ) a spanwise spacing of ( $y_n$ ) and the insert is separated from the blade wall by a distance ( $z_n$ ). The cooling air, after passing through the orifices and impinging on the blade surface is constrained to flow in the chord wise direction and is discharged at the trailing edge flow from the upstream jets in the array, therefore impose a crossflow on those located downstream, [4].

2- Specifying the boundary conditions. Along the external profile (hot gas side), the heat transfer coefficient varies in the manner shown in Figure (3) with the hot gas temperature taken to be uniform and equal to (963K) around the blade external profile for all cases, these are described by Walker, [4 ]

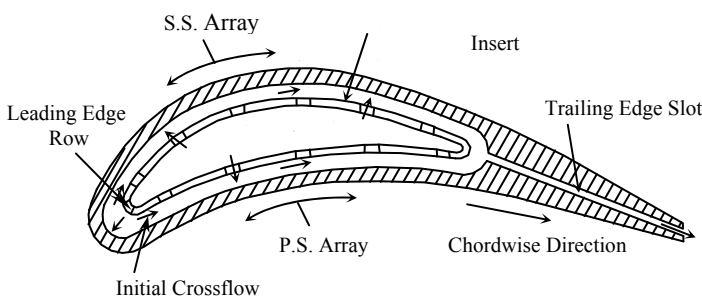


**Figure (1) Blade Geometry**

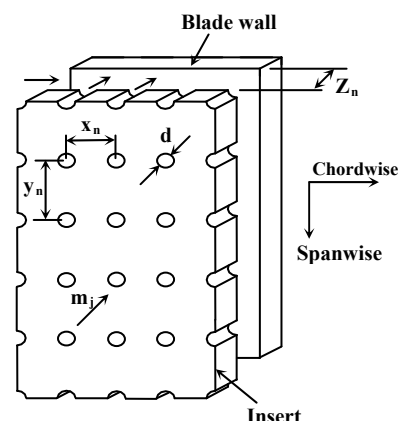


**Figure (2) Detail of S.S. and P.S. Arrays**

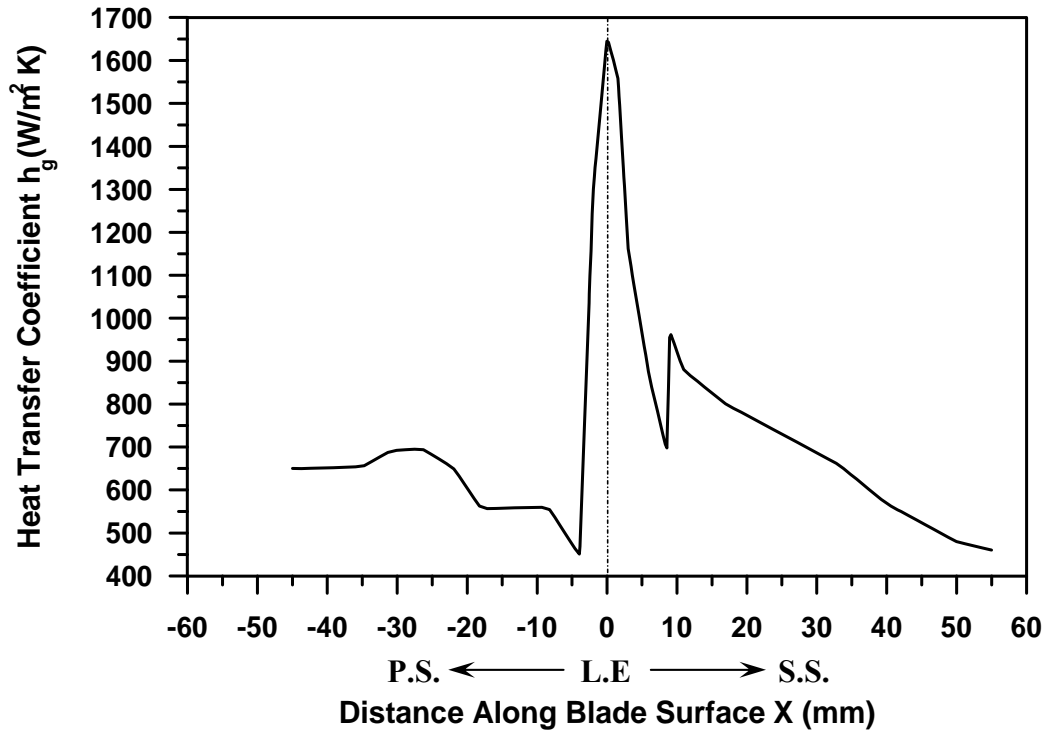


Figure (3) The Variation of the External Heat Transfer Coefficient,[4]

#### GRID GENERATION

Grid generation technique can be roughly classified into three categories:

1. Complex variables methods.
2. Algebraic methods.
- 3- Differential equation techniques.

Only the third category is suitable for the present case because of the complex shape. In this technique, elliptic PDE's has been used to generate grids.

This choice can be better understood by considering the solution of a steady heat conduction problem in two dimensions. The solution of this problem produces isotherms, which are smooth and non-intersecting.

Thompson, [10], worked extensively on using elliptic PDE's to generate grids. This procedure is similar to that used by Hoffman, [11], and transforms the physical plane into the computational plane where the mapping is controlled by a Poisson's equation. This mapping is constructed by specifying the desired grid points (x,y) on the boundary of the physical domain. The distribution of points on the interior is then determined by solving the following equations,

$$\xi_{xx} + \xi_{yy} = P(x, y) \quad (1)$$

$$\eta_{xx} + \eta_{yy} = Q(x, y) \quad (2)$$

Where  $(\xi, \eta)$  represents the coordinate in the computational domain and  $(P, Q)$  are terms which control the point spacing on the interior of physical domain. Where for Laplace equation,[8] Let us assume:

$$\xi = \xi(x, y) \quad (3)$$

$$\eta = \eta(x, y) \quad (4)$$

Differentiating partially each of the equations (3 and 4) with respect to  $\xi$  and  $\eta$  respectively, we get

$$\begin{aligned} \xi_x &= J^{-1}y_\eta \\ \xi_y &= -J^{-1}x_\eta \\ \eta_x &= -J^{-1}y_\xi \\ \eta_y &= J^{-1}x_\xi \end{aligned} \quad (5)$$

Where  $J^{-1}$  is defined by equation (6)

$$J^{-1} = 1/(x_\xi y_\eta - x_\eta y_\xi) \quad (6)$$

The resultant transformed of equations (1) and (2) are

$$ax_{\xi\xi} - 2bx_{\xi\eta} + cx_{\eta\eta} = -J^2(Px_\xi + Qx_\eta) \quad (7)$$

$$ay_{\xi\xi} - 2by_{\xi\eta} + cy_{\eta\eta} = -J^2(Py_\xi + Qy_\eta) \quad (8)$$

Where,

$$a = x_\eta^2 + y_\eta^2$$

$$b = x_\xi x_\eta + y_\xi y_\eta$$

$$c = x_\xi^2 + y_\xi^2$$

For  $P=Q=0$ , equations (7 and 8) become in terms of central finite difference, [12]

$$\begin{aligned} a_{i,j} \left[ \frac{x_{i+1,j} - 2x_{i,j} + x_{i-1,j}}{\Delta\xi^2} \right] - 2b_{i,j} \left[ \frac{x_{i+1,j+1} - x_{i+1,j-1} - x_{i-1,j+1} + x_{i-1,j-1}}{4(\Delta\xi)(\Delta\eta)} \right] \\ + c_{i,j} \left[ \frac{x_{i,j+1} - 2x_{i,j} + x_{i,j-1}}{\Delta\eta^2} \right] = 0 \end{aligned} \quad (9)$$

$$\begin{aligned} a_{i,j} \left[ \frac{y_{i+1,j} - 2y_{i,j} + y_{i-1,j}}{\Delta\xi^2} \right] - 2b_{i,j} \left[ \frac{y_{i+1,j+1} - y_{i+1,j-1} - y_{i-1,j+1} + y_{i-1,j-1}}{4(\Delta\xi)(\Delta\eta)} \right] \\ + c_{i,j} \left[ \frac{y_{i,j+1} - 2y_{i,j} + y_{i,j-1}}{\Delta\eta^2} \right] = 0 \end{aligned} \quad (10)$$

Both of equations (9) and (10) can be solved easily by the Gauss-Siedel iterative method,

To start the solution, an initial distribution of  $x$  and  $y$  coordinates of the grid points within the physical domain must be provided by using an algebraic model, and this coordinates ( $x, y$ ) are used as initial values to solve both of equation (9) and (10). The resultant mesh is shown in Figure (4).

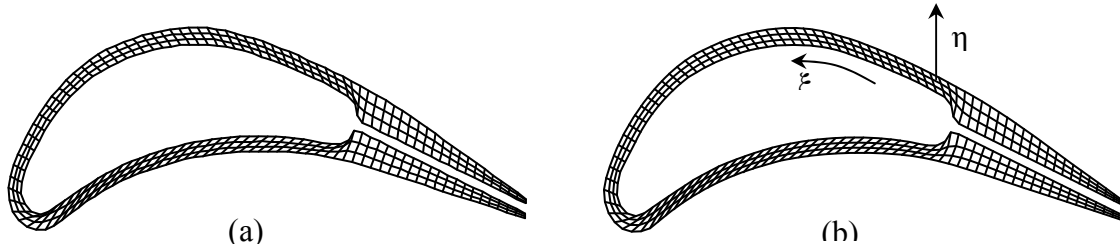


**Figure (4) (a) Algebraic Grid Generation  
(b) Two-Dimensional Grid in Physical Plane**

From Figure (4) there is clearly a high degree of skewness in some regions of the domain. This skewness will cause some difficulty and inaccuracy in the computation of the normal gradients of the temperature at the surface.

So, Poisson’s equation was selected to achieve orthogonality of the grid lines at the surface, these are described by Hoffmann, [11].

The source terms can be evaluated in a manner based on normal intersection between the boundary and grid lines.

They have the form, showed by ref. [13]

$$P = \phi(\xi, \eta)(\xi_x^2 + \xi_y^2) \tag{11}$$

$$Q = \psi(\xi, \eta)(\eta_x^2 + \eta_y^2) \tag{12}$$

Substituting in equation (7) and (8) both of this equation can be written as:

$$a(x_{\xi\xi} + \phi x_{\xi\xi}) - 2bx_{\xi\eta} + c(x_{\eta\eta} + \psi x_{\eta\eta}) = \tag{13}$$

$$a(y_{\xi\xi} + \phi y_{\xi\xi}) - 2by_{\xi\eta} + c(y_{\eta\eta} + \psi y_{\eta\eta}) = \tag{14}$$

Where  $\phi$  and  $\psi$  are specified through the boundary conditions.

$$\phi = \frac{-(x_{\xi}x_{\xi\xi} + y_{\xi}y_{\xi\xi})}{(x_{\xi}^2 + y_{\xi}^2)} \quad \text{on } \eta = \eta_b \tag{15}$$

$$\psi = \frac{-(x_{\eta}x_{\eta\eta} + y_{\eta}y_{\eta\eta})}{(x_{\eta}^2 + y_{\eta}^2)} \quad \text{on } \xi = \xi_b \tag{16}$$

The parameters  $\phi$  and  $\psi$  are calculated at each mesh point in the boundary, then its value at interior mesh points can be computed by linear interpolation.

Gauss Siedel method is used to solve equations (13) and (14). This application will give us a new grid shown in Figure (5)

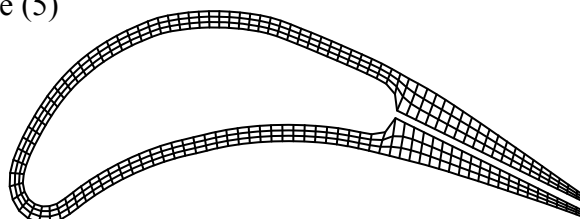


**Figure (5) Orthogonal Grid Generation**

**TRANSFORMATION OF GOVERNING HEAT TRANSFER EQUATIONS:-**

The next step in this work is the transformation of governing heat transfer equations (conduction, convection). For steady-state, two dimensional, the basic equation for temperature field can be written as:

$$\frac{\partial^2 T}{\partial x^2} + \frac{\partial^2 T}{\partial y^2} = 0 \quad (17)$$

The two partial derivatives will be transformed to a new computational domain as follows:

$$\frac{\partial^2 T}{\partial x^2} = \xi_x^2 T_{\xi\xi} + 2\xi_x \eta_x T_{\xi\eta} + \eta_x^2 T_{\eta\eta} + \xi_{xx} T_{\xi} + \eta_{xx} T_{\eta} \quad (18)$$

$$\frac{\partial^2 T}{\partial y^2} = \xi_y^2 T_{\xi\xi} + 2\xi_y \eta_y T_{\xi\eta} + \eta_y^2 T_{\eta\eta} + \xi_{yy} T_{\xi} + \eta_{yy} T_{\eta} \quad (19)$$

By substitution both of equations (18) and (19) in equation (17) this equation becomes,

$$\begin{aligned} & (\xi_x^2 + \xi_y^2) T_{\xi\xi} + 2(\xi_x \eta_x + \xi_y \eta_y) T_{\xi\eta} + (\eta_x^2 + \eta_y^2) T_{\eta\eta} \\ & + (\xi_{xx} + \xi_{yy}) T_{\xi} + (\eta_{xx} + \eta_{yy}) T_{\eta} = 0 \end{aligned} \quad (20)$$

This equation can be applied to the interior nodes to get the temperature distribution in these nodes and can be solved by Gauss- Siedel iterative method, with central difference approximation we get :

$$\begin{aligned} T_{i,j} = & \left\{ \frac{a_1}{\Delta\xi^2} (T_{i+1,j} + T_{i-1,j}) + \frac{b_1}{2\Delta\xi\Delta\eta} (T_{i+1,j+1} - T_{i+1,j-1} - T_{i-1,j+1} \right. \\ & + T_{i-1,j-1}) + \frac{c_1}{\Delta\eta^2} (T_{i,j+1} + T_{i,j-1}) + \frac{d_1}{2\Delta\xi} (T_{i+1,j} + T_{i-1,j}) \\ & \left. + \frac{e_1}{2\Delta\eta} (T_{i,j+1} + T_{i,j-1}) \right\} / \left( \frac{2a_1}{\Delta\xi^2} + \frac{2c_1}{\Delta\eta^2} \right) \end{aligned} \quad (21)$$

For surface nodes (outer and inner) where convective boundary condition is applied, the transformation applied to the distances between nodes along the blade in order to be acceptable for using in determining the temperature distribution in these nodes.

The distance along the blade as shown in Fig.(6) is :

$$s = \sqrt{dx^2 + dy^2} \quad (22)$$

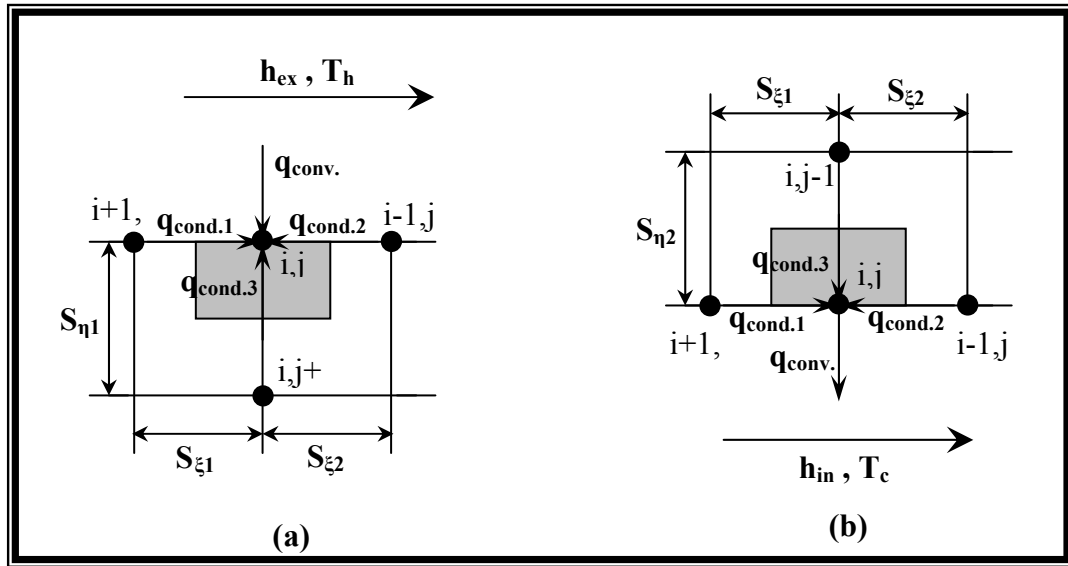


Fig. (6) a- Analysis for External Surface Nodes  
 b- Analysis for Internal Surface Nodes

The energy equation for the surface nodes can be written as:

$$q_{conduction} = q_{convection} \tag{23}$$

For external surface nodes see fig. (6-a) the equation (23) becomes

$$-K\left(\frac{S_{\eta 1}}{2}\right)T_{\xi 1}-K\left(\frac{S_{\eta 1}}{2}\right)T_{\xi 2}-K\left(\frac{S_{\xi 1}+S_{\xi 2}}{2}\right)T_{\eta 1}=h_{ex}\left(\frac{S_{\xi 1}+S_{\xi 2}}{2}\right)\left(T_{\infty}-T_{i,j}\right) \tag{24}$$

So this equation can be solved by Gauss- Siedel iterative method, to get :

$$T_{i,j}=\frac{l}{a 2+b 2+c 2+d 2}\left\{a 2 T_{i,j+1}+b 2 T_{i+1,j}+c 2 T_{i-1,j}+d 2 T_h\right\} \tag{25}$$

Similarly, for the internal surface nodes see figure (6 b) the equation (23) becomes,

$$-K\left(\frac{S_{\eta 2}}{2}\right)T_{\xi 1}-K\left(\frac{S_{\eta 2}}{2}\right)T_{\xi 2}-K\left(\frac{S_{\xi 1}+S_{\xi 2}}{2}\right)T_{\eta 2}=h_{in}\left(\frac{S_{\xi 1}+S_{\xi 2}}{2}\right)\left(T_{i,j}-T_{\infty}\right) \tag{26}$$

So this equation after rearrangement becomes,

$$T_{i,j}=\frac{l}{a 3+b 3+c 3-d 3}\left\{a 3 T_{i,j-1}+b 3 T_{i+1,j}+c 3 T_{i-1,j}-d 3 T_c\right\} \tag{27}$$

This equation are solved by Gauss-Siedel iterative method with central differences for all derivatives except at the surface nodes. The solution of the equations using Gauss-Siedel method requires a design of a computer program, which serves to complete the iterations for all nodes and to give the final solution. This program uses

equations (21), (25) and (27) with a boundary conditions and also the coordinates of the outer, inner and interior points are taken from Figure. (5).

**CONVERGENCE CRITERIE**

The Gauss-Seidel iterative solution continues until specified convergence criterion is met. For this purpose the total changes in the dependent variables are evaluated as, these are described by Hoffmann, [11].

$$Error W = \sum_{\substack{j=j \max-1 \\ i=i \max-1 \\ i=2 \\ j=2}}^{j=j \max-1} ABS[W_{i,j}^{n+1} - W_{i,j}^n] \quad (28)$$

Where W represents quantity of interest (T, x and y) and n represents the iterative level. The convergence criteria is set as error < error-max where error-max is a specified input. In the present study, the error-max is taken as 0.001

The number of nodes that the temperature distribution will be predicted on it is (496) with (I=124 and J=4), and hence, 496 equations must be solved to get the temperature distribution on the blade. To solve these equations, Gauss-Siedel iterative method can be used to get the solution for this system of equations with the help of computer program which serves to give the temperature distribution with 500 iteration.

**CASE STUDIES:-**

**Analysis No. (1):**

Turbine Blade Cooling with Impingement-and Trailing Edge Ejection Based on the Turbulent Flow Between Two Parallel Plates

The insert is perforated by (120) jet orifices and is separated from the hot blade surface by a distance of (1mm). Each of the (120) jet orifices are of (1mm) and arranged into (12) rows of (10) orifices each, i.e., each row consists of (10) orifices in the span wise direction. The rows are arranged so that (6) rows cool the blade suction surface and (5) rows cool the pressure surface as shown in figure (2). For this (11) rows the chord wise spacing ( $x_n$ ) is equal to (5) jet orifice of diameters (5mm), while the spanwise jet spacing ( $y_n$ ) is equal to (8) orifice diameters (8mm). This jet impingement array will be identified as F (5,8) where (5) refers to the chord wise spacing, and (8) to the span wise spacing and the letter (F) to the source of the heat transfer correlation used to describe the array by Florschuetz [14] and [15]. The remaining row is located at the leading edge. The trailing edge region consists of (0.6mm) wide slot which is (80mm) high, (in the spanwise direction). The cooling air mass flow rate is taken as  $28.7 \times 10^{-3}$  Kg/s, all of which passes through the insert and through the jet orifices to form the cooling jets but only half of it,  $14.35 \times 10^{-3}$  Kg/s, passes through the trailing edge slot

For the internal surfaces three distinct regions can be considered;

**(A) The Leading Edge Region**

Chupp *et al.*, [16], investigated the heat transfer at a simulated internal leading edge region of a turbine blade cooled by a single row of impinging air jets. The results of this experimental work consist of two heat transfer correlations. One for the jet stagnation region and one for the area around the jet stagnation region. These two correlations will be used here to characterize the heat transfer coefficients in this region. The mass flow rate through the leading edge row,  $\dot{m}_i$ , is taken as  $2.392 \times 10^{-3}$

Kg/s, which is one twelfth of the total coolant mass flow rate,  $\dot{m}_c$ . From Ref. [16] the spanwise averaged Nusselt Number for the jet stagnation region was correlated from the experimental results to be;

$$Nu_{stag} = 0.44 Re_j^{0.7} \left(\frac{d}{y_n}\right)^{0.8} \exp\left[-0.85\left(\frac{d_s}{d}\right)\left(\frac{d}{y_n}\right)\left(\frac{d}{d_{le}}\right)^{0.4}\right] \quad (29)$$

Where  $Re_j$  is the jet Reynolds number,  $d_{le}$  is the leading edge diameter and  $d_s$  is the distance between the insert and the leading edge blade wall, where  $Re_j = 13739, d = 1mm, d_{le} = 3.6mm, d_s = 2mm, y_n = 8mm$

Hence from equation (29);  $Nu_{stag} = 58, h_{stag} = 1825 W/m^2 K$

Around the stagnation region, Chupp et al, [16] established another correlation to found the averaged Nusselt Number from experimental results to be;

$$Nu_{asg} = 0.63 Re_j^{0.7} \left(\frac{d}{y_n}\right)^{0.5} \left(\frac{d}{d_{le}}\right)^{0.6} \exp\left[-1.27\left(\frac{d_s}{d}\right)\left(\frac{d}{y_n}\right)^{0.5} \left(\frac{d}{d_{le}}\right)^{1.2}\right] \quad (30)$$

From which it can be calculated;  $Nu_{asg} = 67, h_{asg} = 2121 W/m^2 K$

With the heat transfer coefficient determined for the leading edge region it only remains to specify the fluid temperatures in these areas ( $T_{stag}$ ) and ( $T_{asg}$ ) and these were both taken as (378K).

### B) The Pressure and Suction Surface Jet Arrays

The interior surface of the blade along the pressure and suction surfaces are cooled by (5) and (6) rows of jets respectively.

The heat transfer coefficients for the suction surface can be calculated using the correlation developed by Ref. [15]. The correlation is based on experimental results, the Nusselt Number resolved to one chordwise jet spacing is,

$$Nu_a = A_1 Re_j^m \left[1 - A_2 \left[\left(\frac{Z_n}{d}\right)\left(\frac{G_c}{G_j}\right)\right]^r\right] Pr^{0.333} \quad (31)$$

Where,  $A_1 = 0.67, A_2 = 0.237, m = 0.719$  and  $r = 0.317$

$$Re_j = \frac{G_j d}{\mu}$$

The calculated values of heat transfer coefficients are shown in table (1) in terms of the distance of jet spacing (x) along the blade surface.

Along the blade wall, (the impingement surface), the heat flux can be defined as:

$$q'' = h_a (T_s - T_{aw}) \quad (32)$$

Where ( $T_{aw}$ ) is the adiabatic wall temperature and can be defined in a non-dimensional effectiveness, ( $E_T$ ) as:

$$E_T = \frac{T_{aw} - T_j}{T_i - T_j} \quad (33)$$

Where,  $T_j$ : is the jet temperature,  $T_i$ : is the temperature of the initial cross flow,  $T_i > T_j$

The driving fluid temperature along the array ( $T_a$ ) can be taken as ( $T_{aw}$ ) hence once ( $E_T$ ) is known ( $T_a$ ) can be found. Florschuetz [14] estimates the values of ( $E_T$ ) for

an F(5,8) array and represented in table (1) together with the calculated values of ( $T_a$ ), where ( $T_j$ ) was taken as (378K) and ( $T_i$ ) as (477K).

For the pressure surface, the heat transfer coefficients are calculated according to equation (31) for which only  $Re_j$  and  $G_c/G_j$  will change and the results are listed in table (2). The value of ( $E_T$ ) reflects the influence of the higher temperature of the initial cross flow from the leading edge and because the ratio of the initial cross flow to the impingement jet array flow,  $M$ , has increased from 0.083 to 0.1, different ( $E_T$ ) values exist for the pressure surface. These values, together with the calculated values of ( $T_a$ ) based on a ( $T_i$ ) of (477K) and ( $T_j$ ) of (378K) as before, are shown in table (2).

Table (1) Result of Suction-Surface Heat Transfer Coefficients and Coolant Temperatures Obtained From Equations (31) and (33)

x(mm)	$h_a$ (W/m <sup>2</sup> K)	$E_T$	$T_a$ (K)
0 – 5	1581	0.258	403.5
5 – 10	1531	0.220	399.8
10 – 15	1514	0.198	397.6
15 – 20	1516	0.166	394.5
20 – 25	1540	0.120	389.9
25 – 30	1559	0.100	387.9

Table (2) Result of Pressure-Surface Heat Transfer Coefficients and Coolant Temperatures Obtained From Equations (31) and (33)

x(mm)	$h_a$ (W/m <sup>2</sup> K)	$E_T$	$T_a$ (K)
0 – 5	1601	0.278	405.5
5 – 10	1550	0.219	399.7
10 – 15	1533	0.182	396
15 – 20	1536	0.135	391.4
20 – 25	1552	0.106	388.5

**(c) The Trailing Edge Slot**

The average slot cooling air temperature is calculated according to the equation

$$T_{slot} = \frac{T_{sin} + T_{sout}}{2} \tag{34}$$

From Ref. [10], we found that,  $T_{sin} = 443k$ ,  $T_{sout} = 471k$

so from equation (34),  $T_{slot} = 458k$

From Ref. [17], the heat transfer coefficients were determined according to a correlation based on a turbulent flow between parallel plates:

$$Nu_{slot} = Nu_{fs} / (1 - C_T) \tag{35}$$

Where  $Nu_{fs}$ : is the nusselt number obtained from the fundamental solutions and  $C_T$ : is an influence coefficient.

From Rohsenow, et al [17] the values of  $Nu_{fs}$  and  $C_T$  are given for the distance along the slot. The result is shown in table (3) where (x) is the distance along the slot

Table (3) Results of Trailing Edge Slot Heat Transfer Coefficients Obtained from Equation (35).

x(mm)	$h_{slot}$ (W/m <sup>2</sup> K)
1	1651
1.5	1383
5	1249
15	1233

Analysis No. (2):

### Impingement Cooling Heat Transfer Correlations Based on Square Jet Array.

This analysis uses the same correlation as used in analysis (1), the only changes made are to the geometry, where the insert changed from a (5,8) array to a (5,5) array i.e.; the spanwise and chordwise spacing of the jet orifices were equal. This reduction in jet orifice spacing for all (12) rows results in an increase from (120) to (192) jet orifices i.e.; each row consists of (16) orifices in the span wise direction.

#### (A) The Leading Edge

The heat transfer coefficient is found to differ from that obtained in the previous analyses due changes in the span wise spacing of the jet orifices from (8) to (5), and therefore this value of heat transfer coefficient according to equation (29) is:

$$h_{stag} = 1773 W / m^2 K$$

Likewise, the heat transfer coefficient in the area around the stagnation region is calculated according to equation (30) to be:  $h_{asg} = 1834 W / m^2 K$

The coolant temperature in these regions,  $T_{stag}$  and  $T_{asg}$ , are again taken as (378K).

#### (B) The Pressure and Suction Surface Jet Arrays

The heat transfer coefficients are calculated according to equation (31) where due to the change in jet spacing, The parameters  $A_1, A_2, m$  and  $r$  now become;

$A_1 = 0.0919$ ,  $A_2 = 0.2636$ ,  $m = 0.7085$ ,  $r = 0.2393$ . The change in array geometry results in different values of effectiveness ( $E_T$ ) pertaining along the array. The values of ( $E_T$ ) are taken from Ref. [42]. The values of ( $T_a$ ) are calculated using equation (29) based on ( $T_j = 378 K$ ) and ( $T_i = 474 K$ ) The heat transfer coefficients and the values of ( $T_a$ ) along the pressure surface can be determined in the same procedure as for the suction surface. The results of this determination are shown in figure (11)

#### (c) The Trailing Edge Slot

The boundary conditions for the slot will be based on the turbulent flow between parallel plates as used in analysis (1).

#### Analysis No. (3):

#### Turbine Blade Cooling with Impingement and Film Cooling

In the previous analyses the impingement jets methods are used to cool the hot blade surfaces. These methods can, however be classified as internal methods of blade cooling, that is the cooling is achieved by the circulation of cooling air within the blade. The cooling requirements and stresses would be less severe if the heat transfer from the hot gas to the blade could be decreased by the process known as film cooling. Film cooling blades are not only cooled by convection, impingement methods, but they are also shielded from the outer hot gas with a film of spent cooling air ejected through the blade surface by rows of holes. The purpose of this analysis to determine the blade temperature distribution for such a film cooled blade. The cooling of the blade will consist of the same internal arrangement as utilized in analysis (1), that is an F(5,8) impingement jet array but in addition film cooling of the outer surface will be achieved through the use of (12) rows of (0.52 mm) diameter ejection holes distributed around the suction and pressure surfaces of the blade. Internally, the geometry remains unchanged from analysis (1). There are (120) jet orifices of (1mm) diameter whose jets impinge on the hot blade surfaces and which are arranged in (12) rows of (10) jets each, these are showed by Ref. [4] Over the suction and pressure surface jet arrays the jets

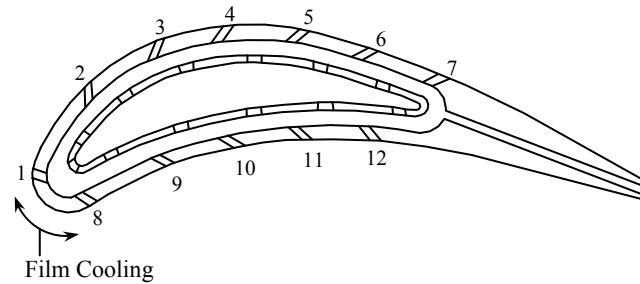


**Fig. (7) Blade Geometry**

are ordered with a spacing of (5) jet orifice diameters in the chord wise direction and (8) in the span wise direction. One half of the spent cooling air from these jets flows rearwards towards the trailing edge and exits the blade through the trailing slot as in analysis (1). The remaining spent cooling air exits the blade through a series of film cooling ejection holes distributed throughout the blade wall. There are in total (468) film cooling holes of (0.52mm) diameter. These are arranged in (12) rows each containing (39) holes each. (7) of the rows are spaced along the suction surface while (5) are spaced along the pressure surface. Within each row the holes are spaced a distance of (2mm) apart. The film cooling holes consist of two rows with an ejection angle of  $64^{\circ}$ , rows 1 and 8 and 10 rows with an ejection angle of  $45^{\circ}$ .

#### Specification of Boundary Conditions

The specification of the boundary conditions can be sub-divided into two main areas:

1-The internal boundary conditions, which will be dealt with in a similar manner to that used in analysis (1), as the internal cooling arrangement and geometry remains unaltered from this analysis.

2-The external boundary conditions, which must take into account the presence of the ejected cooler film of air over the outer surface of the blade.

#### Internal Boundary Conditions

The boundary conditions at the leading edge are unaltered from analysis (1), Likewise the heat transfer coefficients for the suction and pressure surfaces jet arrays also remain unchanged

However the value of  $T_{a_s}$ , the array driving temperature does change because the temperature of the initial cross flow,  $T_i$  is reduced due to the effect of film cooling in reducing the heat transfer to the blade. The trailing edge slot conditions also change because the temperature of the cooling air entering the slot,  $T_{sin}$  is reduced again because of the decrease in heat transfer to the blade.

#### Suction Surface-Coolant Temperatures

The value of  $T_i$ , from a series of preliminary runs was determined to be (465K) which is less than the value obtained in analysis (1) due to the protection obtained from the film cooling which reduces the heat transfer to the blade and consequently to the cooling air.

This value of  $T_i$  is then used in equation (33) to obtain the values of ( $T_a$ ) as shown in figure(13) where ( $E_T$ ) is obtained from analysis (1)

#### Pressure Surface – Coolant Temperatures

Again the initial cross flow temperature,  $T_i$  is reduced to (465 K) and using the same values of  $E_T$  as for analysis (1),  $T_a$  is determined and the results shown in figure(13)

#### The Trailing Edge Slot

The reduction in the heat addition to the cooling air along the jet arrays at the leading edge due to the film cooling reduces the temperature of the coolant entering the slot and hence alters the slot boundary conditions. The boundary conditions are based on the parallel plate flow with the following required parameters;  $T_{sin} = 423 K$ ,  $T_{sout} = 428 K$ ,  $T_{slot} = 425.5 K$

The calculated values of  $h_{slot}$  along the slot are presented in table (4)

Table (4) Results of Trailing Edge Slot- Heat Transfer Coefficients Obtained from Equation (35)

x(mm)	$h_{slot}(W/m^2K)$
1	1673
1.5	1404
5	1282
15	1265

#### External Boundary Conditions

The ejection of cooling air through the film cooling holes results in a change in the conditions existing along the outer profile of the blade. This section seeks to specify the new boundary conditions that now exist as a result of the film cooling used on this blade.

An analysis of the boundary layer with film cooling results in the specification of the heat flux to the blade surface from the hot gas as;

$$q'' = h_{ext}(T_{aw} - T_s) \quad (36)$$

Where  $q''$  is the heat flux to the blade.

$h_{ext}$  is the heat transfer coefficient without film cooling, i.e.; as given by Figure (3).

$T_s$  the blade wall surface temperature,  $T_{aw}$  is the adiabatic wall temperature.

The adiabatic wall temperature can be non-dimensionalized as a film cooling effectiveness,  $E_f$  defined by;

$$E_f = \frac{T_g - T_{aw}}{T_g - T_{c2}} \quad (37)$$

Where  $T_g$  is the gas temperature.

$T_{c2}$  is the temperature of the coolant leaving the film cooling holes, as shown in Figure (8).

the effectiveness ( $E_f$ ) is defined for the  $45^\circ$  and  $64^\circ$  ejection angles as :

$$E_{f_{45}} = 0.3901 / (1 + 0.44 R^{0.8}) \quad (38)$$

$$E_{f_{64}} = 0.3901 / (1 + 0.46 R^{0.8}) \quad (39)$$

Where,

$$R = \left( \frac{x}{1.2 Se} \right) \left[ \text{Re}_{c2} \left( \frac{\mu_{c2}}{\mu_g} \right) \right]^{-0.25} \quad (40)$$

$Se = 0.4084 \text{ mm}$ ,  $\mu_{c2} = 23.8 \times 10^{-6} \text{ kg/m.s}$ ,  $\mu_g = 40.8 \times 10^{-6} \text{ kg/m.s}$ ,  $\text{Re}_{c2} = 3207$

The value of  $T_g$  used in equation (37) varies from row to row because the films from successive rows reinforce each other, i.e.; the film temperature upstream of a row becomes the gas temperature of the next downstream row. Rows (1) and (8), which are the first rows on the suction and pressure surfaces inject the coolant into the external flow which has a temperature of 963K the second rows, i.e.; (2) and (9), inject their coolant into the film provided by rows (1) and (8) which is now at a lower temperature. This reduction in the effective  $T_g$  continues for the other downstream rows also. The effective  $T_g$  used for each row is shown in table (5). This temperature is equal to the value of  $T_{c \text{ film}}$  existing just upstream of the row. For example row (2) is 7.7 mm downstream of row (1). For  $x=7.7 \text{ mm}$ ,  $E_{f64}$  can be calculated to be 0.2028 from which  $T_{c \text{ film}}$  is 853.5 K, based on a  $T_g$  of 963 K. This value of  $T_{c \text{ film}}$  is now used as the effective gas temperature,  $T_g$  for the calculations for the second row.

Table (5) Results of Effective Gas Temperature  
Obtained from Equation (37)

Film Cooling Row	Effective $T_g$ (K)
1	963
2	853.5
3	752
4	669
5	609
6	564
7	529
8	963
9	847
10	742
11	663
12	603

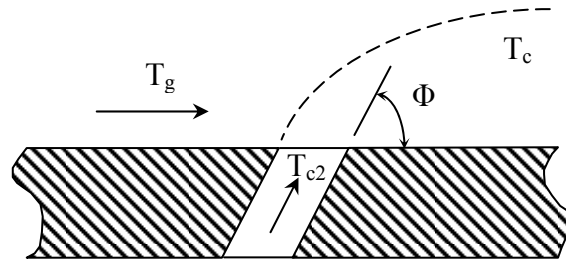


Fig. (8) Film Cooling Hole

## RESULTS AND DISCUSSIONS

Prediction of blade temperature distribution was performed by using three cases, hence three different heat transfer correlation were used.

In the three cases, the blade cooling was assumed to be by using a blade with impingement cooling and trailing edge ejection. The reason behind this choice is that this type of cooling has a wide range of use in practice.

### Analysis No. (1):

The internal boundary conditions for analysis (1) can be summarized in Figure (9), showing the values of the heat transfer coefficient and the fluid temperature associated with each region of the blade.

The temperature contour pattern of Figure (10) shows the maximum temperature of (662 K) at the leading edge region with falling temperatures along both the pressure and suction surfaces followed by a rise in temperature towards the trailing edge. Closer inspection of figure (10) shows that over the pressure surface, from the leading edge, the temperature falls quite rapidly before leveling out and then increasing continuously

towards the trailing edge. However along the suction surface the fall in temperature from the leading edge region is not great, but this reduction extends over a greater length of the blade than that on the pressure surface. However the minimum temperature on the suction surface is approximately (20 K) higher than the minimum temperature on the pressure surface i.e., over the mid-chord regions of the blade, the suction surface is hotter than the pressure surface. At the trailing edge the situation is reversed with the pressure surface hotter than the suction surface.

These differences in temperatures between the two surfaces can be accounted for by a number of factors:

- 1) The blade structure is hollow which reduces the connectivity between the pressure and suction surfaces and hence reduces the tendency to smooth out temperature differences between the two areas.
- 2) As a result of (1) above, the influence of the variation of external heat transfer coefficient is much greater. For example, 8mm along the suction surface (8,S.S.), there is a rapid fall in  $h_{ext}$  which results the reduction in temperature along the suction surface at (8,S.S.). After this point as  $h_{ext}$  begins to fall again the temperature levels also fall. Comparing this to the pressure surface where  $h_{ext}$  falls very quickly from the stagnation point to (5,P.S.), before rising slowly. The temperature variation is seen to mimic this by falling continuously to (5,P.S.). The mid-chord regions also exhibit the effect of  $h_{ext}$ , with the decreasing temperature along the suction surface from (10,S.S.) to (35,S.S.) reflecting the decreasing  $h_{ext}$  while the rise in temperatures along the pressure surface from (18,P.S.) to (28,P.S.) mimicing the rising  $h_{ext}$ .
- 3) The cooler pressure surface can also be accounted for by the higher values of the impingement heat transfer coefficients in this region. The variation of the array heat transfer coefficients does affect the variation of the resulting temperature distribution but because these array variations are much smaller than the variation of  $h_{ext}$  their influence on the temperature variations is consequentially less.
- 4) The trailing edge temperature distribution is more complex than the other blade regions and reflects both the variations of  $h_{ext}$  as well as the varying blade wall thickness around the trailing edge slot. The general increase in temperature towards the trailing edge can also be accounted for by the lower value of  $h_{slot}$  when compared to the impingement values,  $h_a$ .

#### Analysis No. (2):

The internal boundary conditions for this analysis are presented in Figure (11), While the external boundary conditions are the same as in analysis (1)

The results of the thermal analysis are presented in Figure (12) shows a pattern very similar to the analysis (1), (5,8) array with maximum temperature of (688 K) at the leading edge. The temperature levels fall over the mid-chord regions before rising towards the trailing edge. For the purpose of comparing the (5,8) and (5,5) arrays, It is clear that while the pattern remains very similar, the (5,8) case, with less jet orifices produces lower blade temperatures than the (5,5) case which has more jet orifices. This apparent contradiction occurs due to the reduction in  $Re_j$  as the number of orifice increase leading to a reduction in the levels of the heat transfer coefficient. For the trailing edge region of the blade, the difference between the blade surface temperatures is very small reflecting the diminishing influence of changes to the cooling arrangement of the insert and also reflecting the similarity of the boundary conditions along the trailing edge slot.

Analysis No. (3):

Figure (13) shows the internal boundary conditions of analysis (3) when the blade is cooled with film cooling. Figure (14) illustrates the temperature contour pattern within the blade and shows the significant effect that film cooling has on the blade temperatures. Again the highest temperatures occur at the leading edge corresponding to the area of highest ( $h_{ext}$ ) and no film cooling. Across the pressure and suction surfaces the temperatures fall considerably due to the effect of the multiple rows of film cooling and low temperature reach to (430 K).

Due to the lack of the film cooling around the leading edge, the blade temperatures in this region remain nearly high for this analysis, with the film cooling as for analysis (1), without the film cooling. However it is clear that the blade temperature decreases rapidly after this area and results in the film cooled blade as much as (170 K) cooler than the blade without film cooling. The rise in temperature at the trailing edge can be accounted for by a number of factors such as the reducing trailing edge slot heat transfer coefficient together with the reducing value of ( $E_f$ ) over this region as the last row of film cooling holes is located well upstream of this area.

Figure (15) shows comparison between blade surface temperature for the three methods of analyses used in this work and with that obtained in using the finite element method, Ref [4]. It is clear seen that in all analyses the maximum temperature occurs at the leading edge. In the pressure and suction surfaces the temperature decreases followed by a rise in temperature toward the trailing edge.

It is obvious from figure (15) that analysis (3) with the film cooling gives lower temperature distribution than the other analyses. For the remaining analyses without the film cooling, it can be seen that analysis (1) for (5,8) array and trailing edge heat transfer based on plate flow and lower than analysis (2) which has more jet array for the insert geometry i.e.,(5,5) array and trailing edge heat transfer based on plate flow and this figure shows a great similarity between the finite difference and the finite element results, which seems to coincide in most regions along blade surface. The differences between the results of the two methods are due to the differences in the technique of each method as well as the use of transformation theory, which depends on the transformation of curved boundaries of blade profiles into straight lines.

An inspection to the graphs, it can be seen that the difference of the finite difference results from the finite element method is very small. This difference was calculated to be (3.503 %) as maximum value and it falls to (0%) in most regions.

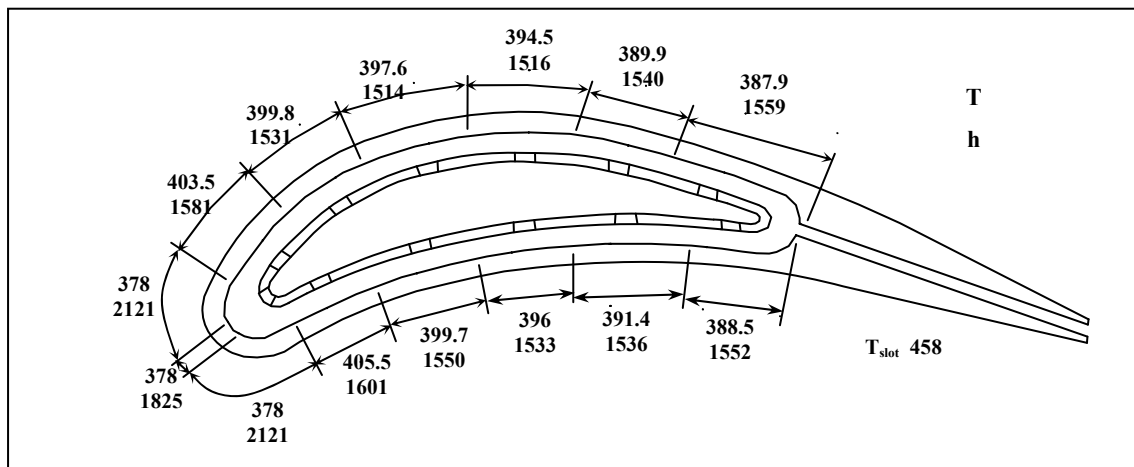


**Figure (9) Internal Boundary Condition-Analysis (1)**

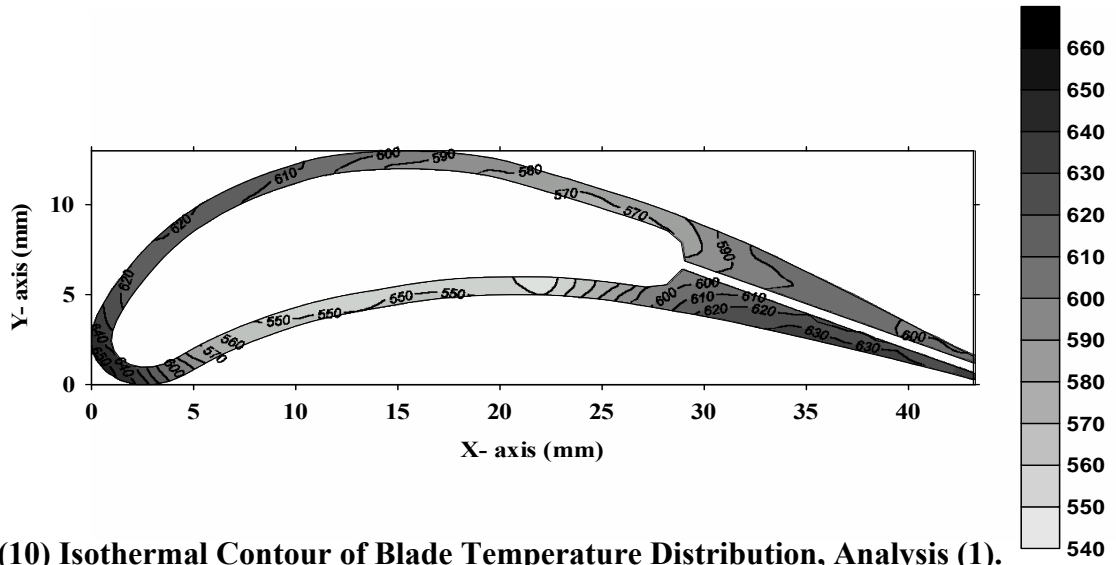


Figure (10) Isothermal Contour of Blade Temperature Distribution, Analysis (1).

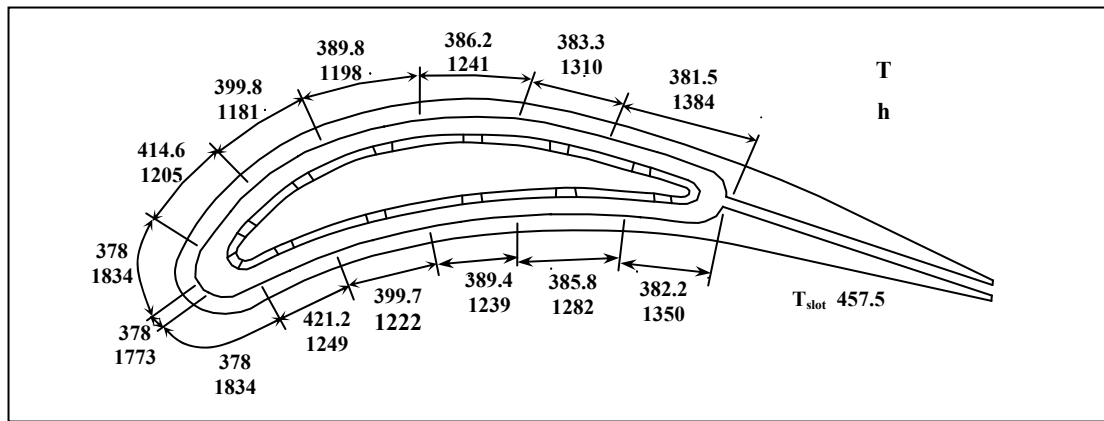


Figure (11) Internal Boundary Condition-Analysis (2)

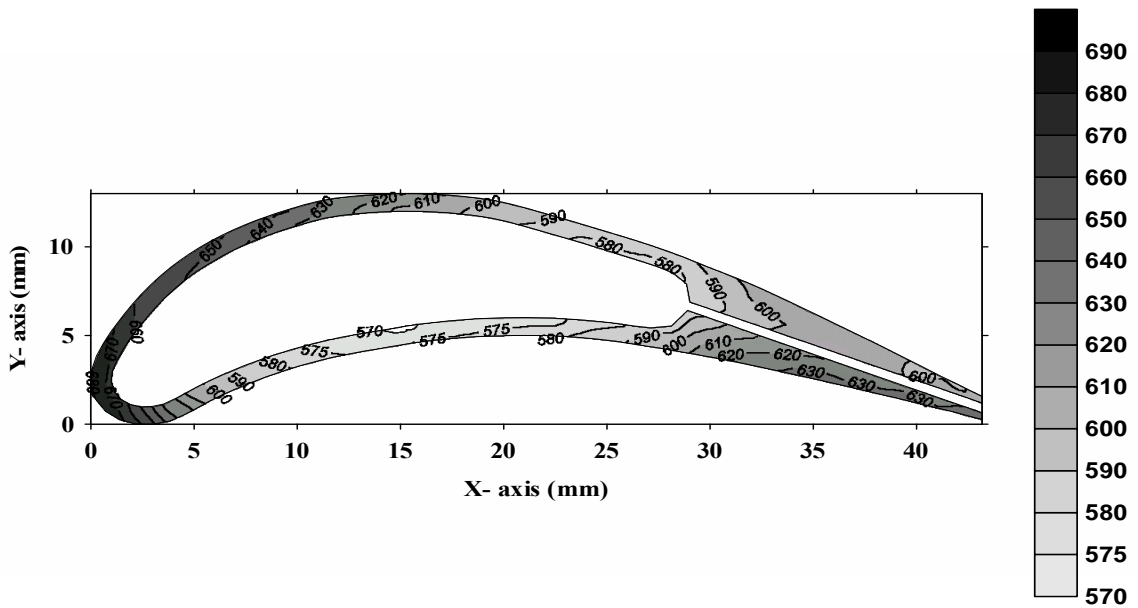


Figure (12) Isothermal Contour of Blade Temperature Distribution, Analysis (2).

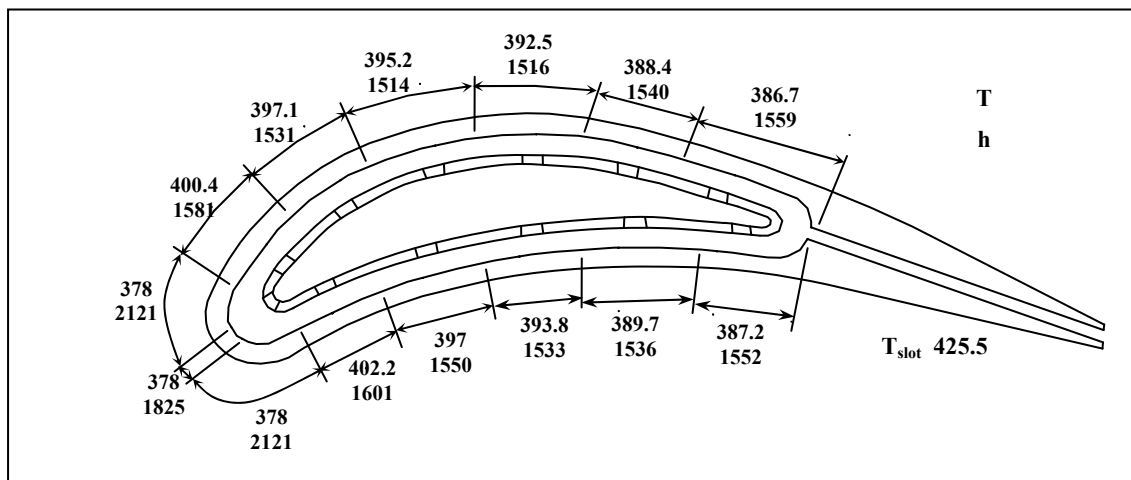


Figure (13) Internal Boundary Condition-Analysis (3)

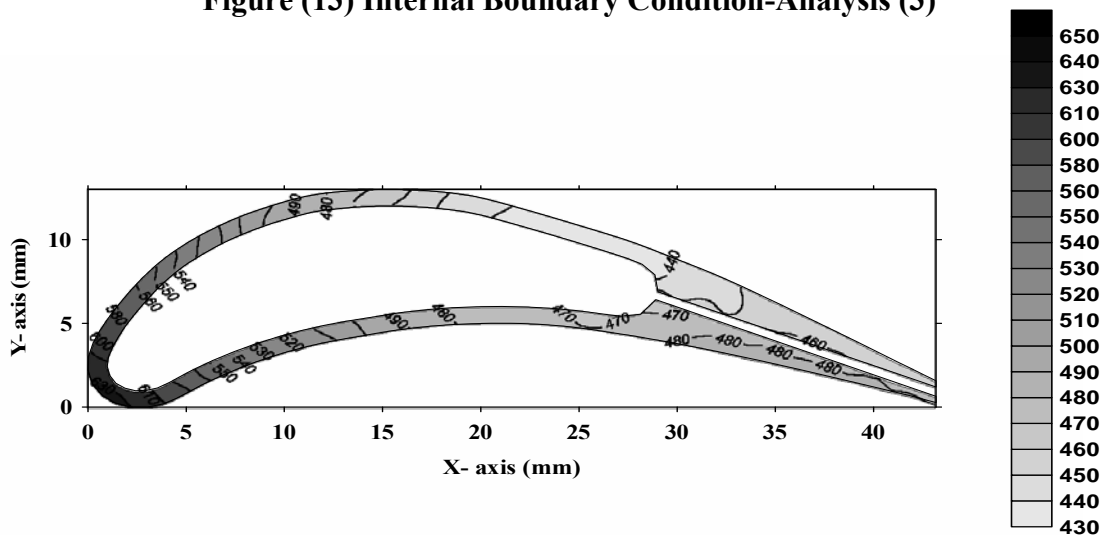


Figure (14) Isothermal Contour of Blade Temperature Distribution, Analysis (3)

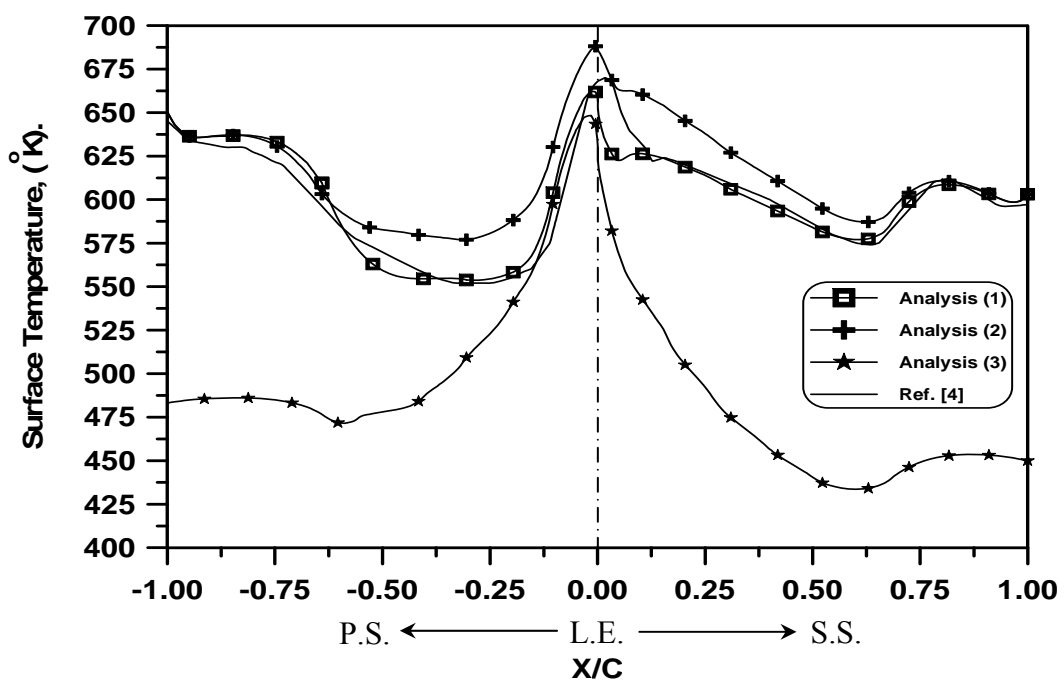


Figure (15) Comparison between Blade Surface Temperature For the Three Analyses and Ref.[4]

## CONCLUSIONS

The main conclusions that can be drawn from this work are summarized in the following points:

1- Three case studies are used for thermal analyses of the blade, which requires the specification of external and internal boundary conditions. It is also found from the results obtained that the best cooling method to the turbine blade have been obtained for the third case when the blade cooled by impingement and film cooling method.

2- The analysis procedure used gave a good results in terms of their accuracy when compared with the results of other researchers.

3- Numerical finite difference was used successfully in obtaining temperature distribution for complicated geometries as compared to the finite element results.

4- The body fitted coordinates method represents an efficient flexible tool for treating difficult geometries.

5- An impingement-cooled blade can be dealt with a two-dimensional thermal analysis through the use of heat transfer correlations, which provide spanwise averaged values of the heat transfer coefficients.

6- The effect of increasing the number of cooling air jets, which impinge on the hot blade surfaces, results in an increase in the blade temperature. This is because the increase in number of jets of high intensity cooling regions is accompanied by a reduction in the jet Reynolds number.

7- Several different heat transfer correlations can be used to describe the impingement jet array areas as they all produce similar values of heat transfer coefficients and hence similar blade temperatures.

8- Film cooling can be analyzed by varying the external boundary conditions of the blade and results in an appreciable reduction in blade temperatures about (170 K) cooler than the blade without film cooling.

## REFERENCES

- [1] El-Wakil, M.M., "Power-Plant Technology", McGraw-Hill, Inc., 1985.
- [2] Turner A.B., Long C.A., Childs P.R. N., Hills N.J., and Millward J.A., "A Review of Some Current Problems in Gas Turbine Systems", [http:\ www.google.com](http://www.google.com), (Key Words "Gas Turbine"), 1998.[Paper]
- [3] Jack D. Mattingly, "Elements of Gas Turbine Propulsion" McGraw-Hill, Inc., 1996.
- [4] Walker M.J.B., "Turbine Blade Internal Heat Transfer", M.Sc. Thesis, Cranfield Institute of Technology, 1989.
- [5] Jaleel J. M., "The Effectiveness of Finite Difference method on Curved Boundary AirCooled Turbine Blades", Journal of Military College of Engineering, No.25, pp. 19-32, 2001.
- [6] Kudor D.S., "Effect of Cooling Air Passage Shape on Gas Turbine Blade Temperature Distribution", M.Sc. Thesis Al-Mustansiria University, Iraq, 2003.
- [7] Marie L.H., Eriksson L.E. and Suden B., "Convective Heat Transfer on an Inlet Guide Vane", [http:\ www.google.com](http://www.google.com), (Key Words "Turbine Blade Cooling"), 2003.[Paper]

- [8] Ken I.T. and Takasago S.A., “Contribution of Heat Transfer to Turbine Blades and Vanes for High Temperature Industrial Gas Turbines”, [http:\ www.google.com](http://www.google.com), (Key Words “Turbine Blade Cooling”), 2000.[Paper]
- [9] Stefan L.F., “Surface Temperature Mapping of Gas Turbine Blading by Means of High Resolution Pyrometry”, [http:\ www.google.com](http://www.google.com), (Key Words “Turbine Blade Cooling”), 2001.[Paper]
- [10] Thompson J.F., “Grid Generation techniques in Computational Fluid Dynamics”, AIAA Journal, Vol.22, No.11, November, pp. 1505-1522, 1984.
- [11] Hoffmann K.A., “Computational Fluid Dynamics for Engineers”, 1989.
- [12] Anderson J.D., “Computational Fluid Dynamics”, McGraw-Hill, Inc., 1995.
- [13] Anderson D.A., John C. Tennehill and Richard H. Pletcher, “Computational Fluid Mechanics and heat Transfer”, McGraw-Hill Company, 1984.
- [14] Florshuetz L.W. Metzger D.E., Su C.C., Isoda Y. and Tseng H.H., “Jet Array Impingement Flow Distribution and Heat Transfer Characteristics-Effect of Initial Crossflow and Nonuniform Array Geometry”, NASA CR 3630, 1982.
- [15] Florshuetz L.W. Metzger D.E. and Truman C.R., “Jet Impingement with Crossflow-Correlation of Streamwise Resolved Flow and Heat Transfer Distributions”, NASA CR 3373, 1981.
- [16] Chupp R.E., Helms H.E., McFadden P.W. and Brown T., “Evaluation of Internal Heat Transfer Coefficients for Impingement- Cooled Turbine Airfoils”, Journal of Aircraft, Vol.6, PP 203-208, 1969.
- [17] Rohsenow W.M., Hartnet J.P. and Ganic E.N., “Handbook of Heat Transfer Fundamentals”, 2<sup>nd</sup> ed. McGraw-Hill Book Co., 1987

NOMENCLATURE

Symbol	Description	Unit
$A_1, A_2$	Correlating Parameters in Equation (31)	–
$d$	Jet Orifice Diameter	mm
$E_f$	Film Cooling Effectiveness	–
$G_j$	Jet Mass Velocity for One Jet Row	kg/m <sup>2</sup> .s
$h_{ex}$	External Heat Transfer Coefficient	W/m <sup>2</sup> . K
$h_{in}$	Internal Heat Transfer Coefficient	W/m <sup>2</sup> . K
$h_{slot}$	Heat Transfer Coefficient of the Slot	W/m <sup>2</sup> . K
$i, j$	The Indexes Increases Along the x and y Axes	–
$J$	Jacobian Transformation	–
$k$	Thermal Conductivity	W/m. K

$Nu$	Nusselt Number	–
$P$	Source Term in Poisson's Equation is Used to Attract $\xi$ -Coordinate lines	–
$Pr$	Prandtl Number	–
$q''$	Heat Flux	W/m <sup>2</sup>
$Q$	Source Term in Poisson's Equation is Used to Attract $\eta$ -Coordinate lines	–
$R$	Correlating Parameter in Equation (41)	–
$S, S_\xi, S_\eta$	Distance Along Blade Surface	mm
$T$	Temperature	K
$T_{aw}$	Adiabatic Wall Temperature	K
$T_\infty$	Fluid (Air) Temperature	K
$x$	Physical Coordinates	mm
$x_n$	Chordwise Spacing	mm
$y$	Physical Coordinates	mm
$y_n$	Spanwise Spacing	mm
$Z_n$	Insert to Blade Wall Distance	mm

Greek Symbol

$\Delta\xi, \Delta\eta$	Spatial Steps in Computational Domain	–
$\phi$	Ejection Angle	Deg.

Abbreviations

P.S.	Pressure Surface
S.S.	Suction Surface

## INTRODUCTION

In order to increase the thermodynamic efficiency of a gas turbine engine, a high turbine inlet temperature is required, [1]. Therefore, the high temperature passing on the turbine blades causes thermal stress to the turbine blades materials. To reduce the effect of thermal stress upon the materials of blade, cooling of blades is required, [2]. The air cooling methods used in the turbine blade can be divided into the following categories, [3]:

1. Convection cooling.
2. Impingement cooling.
3. Film cooling.
4. Full-coverage film cooling.
5. Transpiration cooling.

The purpose of the present study is to find the temperature distribution in air-cooled turbine blades using transformed finite difference equations using body-fitted coordinate system. The work in this paper is divided into two steps, first generating a grid and secondly solving the transformed equations in the new computational coordinates.

There are numbers of numerical, experimental work and theoretical researches in this field to get the best means for improving the increase of the turbine blades operating conditions such as Walker, M.J.B., [4], 1989, introduced a master thesis that involves the determination of temperature distribution within a turbine blade for three configurations of cooled blades (circular, elliptical cooling holes, and cooling with impingement and trailing edge ejection). The determination was by the use of finite element method and for each type, the analysis was demonstrated with different specific boundary conditions and heat transfer correlations. The results are acceptable in terms of their accuracy. This was determined by applying the procedure to a test case and comparing the results with the reference results. Jaleel J.M., [5], 2001, illustrated the finite difference method with suitable approximation for curved boundary to determine the temperature distribution within air-cooled turbine blade utilizing circular cooling holes and verified the effectiveness of the irregular finite difference method on curved non-uniform shapes such as turbine blade. Kuder D.S., [6], 2003, submitted a master thesis that involves the prediction of temperature distribution in gas turbine air-cooled blades from hub to tip. It was achieved through the use of control volume technique. The control volume mesh deals with irregular boundary. Unsteady state two dimensional heat transfer was used to get the temperature distribution. The results of thermal analyses obtained in two case studies in which cooling passages were taken as (15) circular holes, with different diameters and as (3) channel passages. Her results show that the surface temperature distribution with channel cooling passages is (20%) lower than the surface temperature distribution with circular cooling passages. Marie *et al.*, [7], 2003, presented a paper to determine the flow and temperature fields around an inlet guide vane numerically by CFD method. The governing equations are solved by 3D finite-volume Navier-Stokes method. In particular the outer surface temperature, heat transfer coefficient distributions and static pressure distributions are also presented. Ken *et al.*, [8], 2000, investigated experimental tests in a low-speed wind tunnel cascade to determine the film-cooling effectiveness of the film-cooling hole geometry on turbine airfoils. The results of full coverage film-cooling and heat transfer characteristics of rotating serpentine flow passage with and without angled turbulence

promoter had been presented in the full paper. Stefan L.F., [9], 2001, have done an experimental evaluation of both standard and prototype blade designs under real base load conditions by using optical pyrometry. Pyrometry is a valuable tool for the quality assurance, since the temperature distribution of each individual blade is determined carefully. This paper describes the application of a newly developed high-resolution pyrometer to the latest prototype, the V84.3A2 60Hz 180 Mw gas turbine. Thus, using new pyrometer probes in conjunction with a continuous data acquisition mode allows reliable, highly resolved blade surface temperature measurements, where errors and potential risks for the gas turbine are minimized at the same time.

It has been shown from above researches reported here, that their mainly study concentrate on the methods to determine temperature distribution within the blade material. These methods are: analytical, experimental and numerical methods such as control volume, finite element and finite difference method. More progress is needed in present study by using finite difference method with body fitted coordinate system is made to predict the temperature distribution in turbine blade.

**PROBLEM FORMULATION**

The problem specification was taken from a well documented reference source containing the following necessary data:

1- Definition of the blade geometry shown in Figure (1), The blade incorporates an insert which serves as the jet plenum, which is perforated to form array of jet orifices, Figure (2), is giving rise to mid-chord impingement arrays which cool the pressure and suction surfaces and an initial jet orifice row at the blade leading edge. The jet orifices have a diameter ( $d$ ), a chord-wise spacing of ( $x_n$ ) a spanwise spacing of ( $y_n$ ) and the insert is separated from the blade wall by a distance ( $z_n$ ). The cooling air, after passing through the orifices and impinging on the blade surface is constrained to flow in the chord wise direction and is discharged at the trailing edge flow from the upstream jets in the array, therefore impose a crossflow on those located downstream, [4].

2- Specifying the boundary conditions. Along the external profile (hot gas side), the heat transfer coefficient varies in the manner shown in Figure (3) with the hot gas temperature taken to be uniform and equal to (963K) around the blade external profile for all cases, these are described by Walker, [4 ]

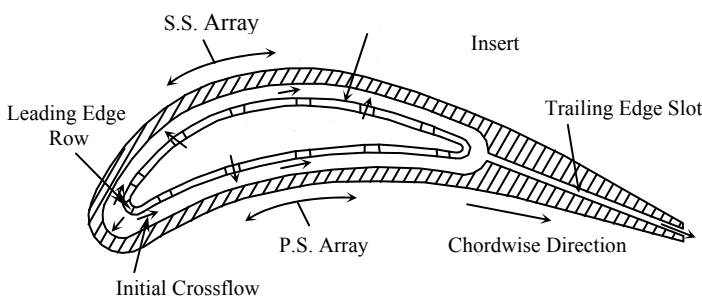


**Figure (1) Blade Geometry**

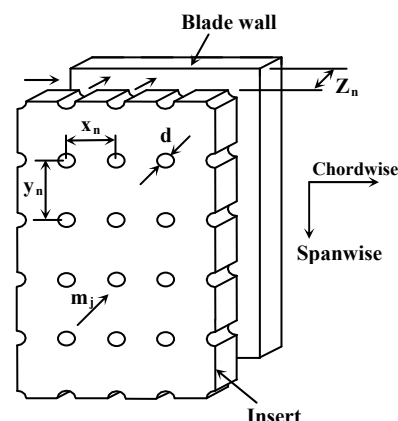


**Figure (2) Detail of S.S. and P.S. Arrays**

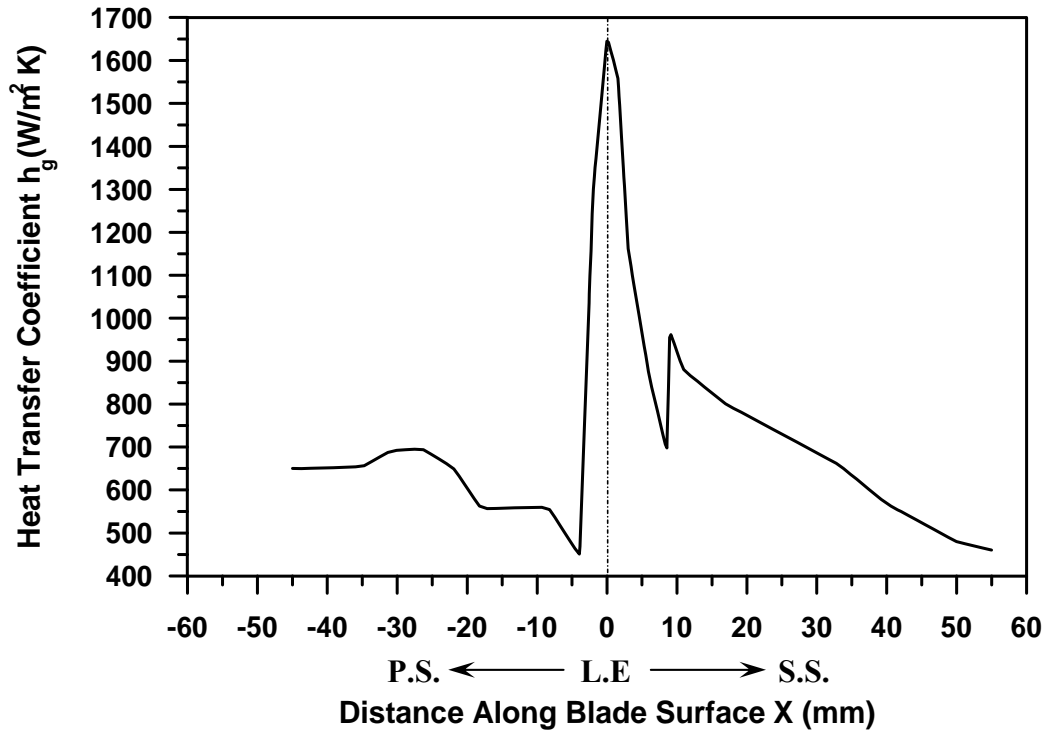


Figure (3) The Variation of the External Heat Transfer Coefficient,[4]

#### GRID GENERATION

Grid generation technique can be roughly classified into three categories:

1. Complex variables methods.
2. Algebraic methods.
- 3- Differential equation techniques.

Only the third category is suitable for the present case because of the complex shape. In this technique, elliptic PDE's has been used to generate grids.

This choice can be better understood by considering the solution of a steady heat conduction problem in two dimensions. The solution of this problem produces isotherms, which are smooth and non-intersecting.

Thompson, [10], worked extensively on using elliptic PDE's to generate grids. This procedure is similar to that used by Hoffman, [11], and transforms the physical plane into the computational plane where the mapping is controlled by a Poisson's equation. This mapping is constructed by specifying the desired grid points (x,y) on the boundary of the physical domain. The distribution of points on the interior is then determined by solving the following equations,

$$\xi_{xx} + \xi_{yy} = P(x, y) \quad (1)$$

$$\eta_{xx} + \eta_{yy} = Q(x, y) \quad (2)$$

Where  $(\xi, \eta)$  represents the coordinate in the computational domain and  $(P, Q)$  are terms which control the point spacing on the interior of physical domain. Where for Laplace equation,[8] Let us assume:

$$\xi = \xi(x, y) \quad (3)$$

$$\eta = \eta(x, y) \quad (4)$$

Differentiating partially each of the equations (3 and 4) with respect to  $\xi$  and  $\eta$  respectively, we get

$$\begin{aligned} \xi_x &= J^{-1}y_\eta \\ \xi_y &= -J^{-1}x_\eta \\ \eta_x &= -J^{-1}y_\xi \\ \eta_y &= J^{-1}x_\xi \end{aligned} \quad (5)$$

Where  $J^{-1}$  is defined by equation (6)

$$J^{-1} = 1/(x_\xi y_\eta - x_\eta y_\xi) \quad (6)$$

The resultant transformed of equations (1) and (2) are

$$ax_{\xi\xi} - 2bx_{\xi\eta} + cx_{\eta\eta} = -J^2(Px_\xi + Qx_\eta) \quad (7)$$

$$ay_{\xi\xi} - 2by_{\xi\eta} + cy_{\eta\eta} = -J^2(Py_\xi + Qy_\eta) \quad (8)$$

Where,

$$a = x_\eta^2 + y_\eta^2$$

$$b = x_\xi x_\eta + y_\xi y_\eta$$

$$c = x_\xi^2 + y_\xi^2$$

For  $P=Q=0$ , equations (7 and 8) become in terms of central finite difference, [12]

$$\begin{aligned} a_{i,j} \left[ \frac{x_{i+1,j} - 2x_{i,j} + x_{i-1,j}}{\Delta\xi^2} \right] - 2b_{i,j} \left[ \frac{x_{i+1,j+1} - x_{i+1,j-1} - x_{i-1,j+1} + x_{i-1,j-1}}{4(\Delta\xi)(\Delta\eta)} \right] \\ + c_{i,j} \left[ \frac{x_{i,j+1} - 2x_{i,j} + x_{i,j-1}}{\Delta\eta^2} \right] = 0 \end{aligned} \quad (9)$$

$$\begin{aligned} a_{i,j} \left[ \frac{y_{i+1,j} - 2y_{i,j} + y_{i-1,j}}{\Delta\xi^2} \right] - 2b_{i,j} \left[ \frac{y_{i+1,j+1} - y_{i+1,j-1} - y_{i-1,j+1} + y_{i-1,j-1}}{4(\Delta\xi)(\Delta\eta)} \right] \\ + c_{i,j} \left[ \frac{y_{i,j+1} - 2y_{i,j} + y_{i,j-1}}{\Delta\eta^2} \right] = 0 \end{aligned} \quad (10)$$

Both of equations (9) and (10) can be solved easily by the Gauss-Siedel iterative method,

To start the solution, an initial distribution of x and y coordinates of the grid points within the physical domain must be provided by using an algebraic model, and this coordinates (x, y) are used as initial values to solve both of equation (9) and (10). The resultant mesh is shown in Figure (4).

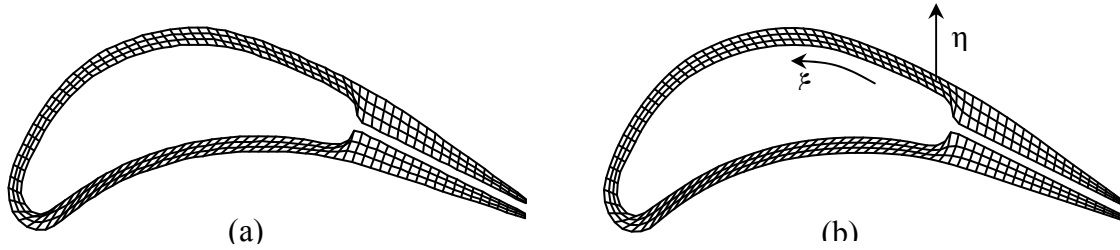


**Figure (4) (a) Algebraic Grid Generation  
(b) Two-Dimensional Grid in Physical Plane**

From Figure (4) there is clearly a high degree of skewness in some regions of the domain. This skewness will cause some difficulty and inaccuracy in the computation of the normal gradients of the temperature at the surface.

So, Poisson’s equation was selected to achieve orthogonality of the grid lines at the surface, these are described by Hoffmann, [11].

The source terms can be evaluated in a manner based on normal intersection between the boundary and grid lines.

They have the form, showed by ref. [13]

$$P = \phi(\xi, \eta)(\xi_x^2 + \xi_y^2) \tag{11}$$

$$Q = \psi(\xi, \eta)(\eta_x^2 + \eta_y^2) \tag{12}$$

Substituting in equation (7) and (8) both of this equation can be written as:

$$a(x_{\xi\xi} + \phi x_{\xi\xi}) - 2bx_{\xi\eta} + c(x_{\eta\eta} + \psi x_{\eta\eta}) = \tag{13}$$

$$a(y_{\xi\xi} + \phi y_{\xi\xi}) - 2by_{\xi\eta} + c(y_{\eta\eta} + \psi y_{\eta\eta}) = \tag{14}$$

Where  $\phi$  and  $\psi$  are specified through the boundary conditions.

$$\phi = \frac{-(x_{\xi}x_{\xi\xi} + y_{\xi}y_{\xi\xi})}{(x_{\xi}^2 + y_{\xi}^2)} \quad \text{on } \eta = \eta_b \tag{15}$$

$$\psi = \frac{-(x_{\eta}x_{\eta\eta} + y_{\eta}y_{\eta\eta})}{(x_{\eta}^2 + y_{\eta}^2)} \quad \text{on } \xi = \xi_b \tag{16}$$

The parameters  $\phi$  and  $\psi$  are calculated at each mesh point in the boundary, then its value at interior mesh points can be computed by linear interpolation.

Gauss Siedel method is used to solve equations (13) and (14). This application will give us a new grid shown in Figure (5)

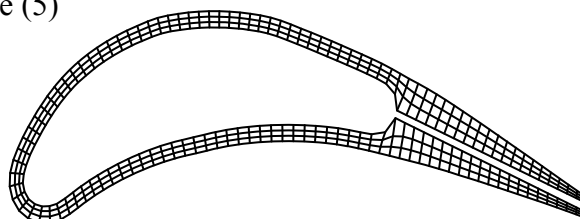


**Figure (5) Orthogonal Grid Generation**

**TRANSFORMATION OF GOVERNING HEAT TRANSFER EQUATIONS:-**

The next step in this work is the transformation of governing heat transfer equations (conduction, convection). For steady-state, two dimensional, the basic equation for temperature field can be written as:

$$\frac{\partial^2 T}{\partial x^2} + \frac{\partial^2 T}{\partial y^2} = 0 \quad (17)$$

The two partial derivatives will be transformed to a new computational domain as follows:

$$\frac{\partial^2 T}{\partial x^2} = \xi_x^2 T_{\xi\xi} + 2\xi_x \eta_x T_{\xi\eta} + \eta_x^2 T_{\eta\eta} + \xi_{xx} T_{\xi} + \eta_{xx} T_{\eta} \quad (18)$$

$$\frac{\partial^2 T}{\partial y^2} = \xi_y^2 T_{\xi\xi} + 2\xi_y \eta_y T_{\xi\eta} + \eta_y^2 T_{\eta\eta} + \xi_{yy} T_{\xi} + \eta_{yy} T_{\eta} \quad (19)$$

By substitution both of equations (18) and (19) in equation (17) this equation becomes,

$$\begin{aligned} & (\xi_x^2 + \xi_y^2) T_{\xi\xi} + 2(\xi_x \eta_x + \xi_y \eta_y) T_{\xi\eta} + (\eta_x^2 + \eta_y^2) T_{\eta\eta} \\ & + (\xi_{xx} + \xi_{yy}) T_{\xi} + (\eta_{xx} + \eta_{yy}) T_{\eta} = 0 \end{aligned} \quad (20)$$

This equation can be applied to the interior nodes to get the temperature distribution in these nodes and can be solved by Gauss- Siedel iterative method, with central difference approximation we get :

$$\begin{aligned} T_{i,j} = & \left\{ \frac{a_1}{\Delta\xi^2} (T_{i+1,j} + T_{i-1,j}) + \frac{b_1}{2\Delta\xi\Delta\eta} (T_{i+1,j+1} - T_{i+1,j-1} - T_{i-1,j+1} \right. \\ & + T_{i-1,j-1}) + \frac{c_1}{\Delta\eta^2} (T_{i,j+1} + T_{i,j-1}) + \frac{d_1}{2\Delta\xi} (T_{i+1,j} + T_{i-1,j}) \\ & \left. + \frac{e_1}{2\Delta\eta} (T_{i,j+1} + T_{i,j-1}) \right\} / \left( \frac{2a_1}{\Delta\xi^2} + \frac{2c_1}{\Delta\eta^2} \right) \end{aligned} \quad (21)$$

For surface nodes (outer and inner) where convective boundary condition is applied, the transformation applied to the distances between nodes along the blade in order to be acceptable for using in determining the temperature distribution in these nodes.

The distance along the blade as shown in Fig.(6) is :

$$s = \sqrt{dx^2 + dy^2} \quad (22)$$

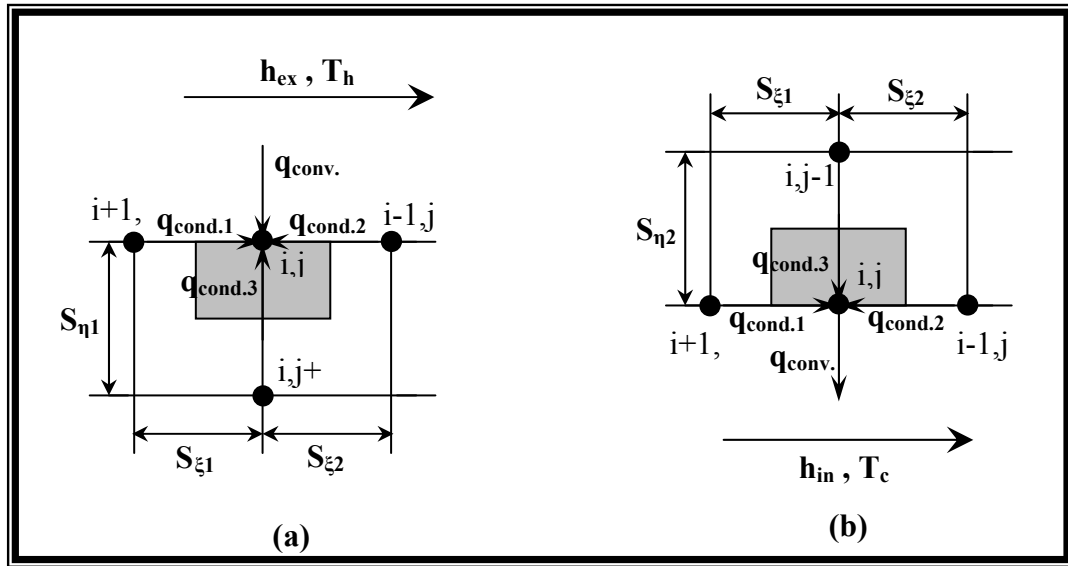


Fig. (6) a- Analysis for External Surface Nodes  
 b- Analysis for Internal Surface Nodes

The energy equation for the surface nodes can be written as:

$$q_{conduction} = q_{convection} \tag{23}$$

For external surface nodes see fig. (6-a) the equation (23) becomes

$$-K\left(\frac{S_{\eta 1}}{2}\right)T_{\xi 1}-K\left(\frac{S_{\eta 1}}{2}\right)T_{\xi 2}-K\left(\frac{S_{\xi 1}+S_{\xi 2}}{2}\right)T_{\eta 1}=h_{ex}\left(\frac{S_{\xi 1}+S_{\xi 2}}{2}\right)\left(T_{\infty}-T_{i,j}\right) \tag{24}$$

So this equation can be solved by Gauss- Siedel iterative method, to get :

$$T_{i,j}=\frac{l}{a 2+b 2+c 2+d 2}\left\{a 2 T_{i,j+1}+b 2 T_{i+1,j}+c 2 T_{i-1,j}+d 2 T_h\right\} \tag{25}$$

Similarly, for the internal surface nodes see figure (6 b) the equation (23) becomes,

$$-K\left(\frac{S_{\eta 2}}{2}\right)T_{\xi 1}-K\left(\frac{S_{\eta 2}}{2}\right)T_{\xi 2}-K\left(\frac{S_{\xi 1}+S_{\xi 2}}{2}\right)T_{\eta 2}=h_{in}\left(\frac{S_{\xi 1}+S_{\xi 2}}{2}\right)\left(T_{i,j}-T_{\infty}\right) \tag{26}$$

So this equation after rearrangement becomes,

$$T_{i,j}=\frac{l}{a 3+b 3+c 3-d 3}\left\{a 3 T_{i,j-1}+b 3 T_{i+1,j}+c 3 T_{i-1,j}-d 3 T_c\right\} \tag{27}$$

This equation are solved by Gauss-Siedel iterative method with central differences for all derivatives except at the surface nodes. The solution of the equations using Gauss-Siedel method requires a design of a computer program, which serves to complete the iterations for all nodes and to give the final solution. This program uses

equations (21), (25) and (27) with a boundary conditions and also the coordinates of the outer, inner and interior points are taken from Figure. (5).

**CONVERGENCE CRITERIE**

The Gauss-Seidel iterative solution continues until specified convergence criterion is met. For this purpose the total changes in the dependent variables are evaluated as, these are described by Hoffmann, [11].

$$Error W = \sum_{\substack{j=j \max-1 \\ i=i \max-1 \\ i=2 \\ j=2}}^{j=j \max-1} ABS[W_{i,j}^{n+1} - W_{i,j}^n] \tag{28}$$

Where W represents quantity of interest (T, x and y) and n represents the iterative level. The convergence criteria is set as error < error-max where error-max is a specified input. In the present study, the error-max is taken as 0.001

The number of nodes that the temperature distribution will be predicted on it is (496) with (I=124 and J=4), and hence, 496 equations must be solved to get the temperature distribution on the blade. To solve these equations, Gauss-Siedel iterative method can be used to get the solution for this system of equations with the help of computer program which serves to give the temperature distribution with 500 iteration.

**CASE STUDIES:-**

**Analysis No. (1):**

Turbine Blade Cooling with Impingement-and Trailing Edge Ejection Based on the Turbulent Flow Between Two Parallel Plates

The insert is perforated by (120) jet orifices and is separated from the hot blade surface by a distance of (1mm). Each of the (120) jet orifices are of (1mm) and arranged into (12) rows of (10) orifices each, i.e., each row consists of (10) orifices in the span wise direction. The rows are arranged so that (6) rows cool the blade suction surface and (5) rows cool the pressure surface as shown in figure (2). For this (11) rows the chord wise spacing ( $x_n$ ) is equal to (5) jet orifice of diameters (5mm), while the spanwise jet spacing ( $y_n$ ) is equal to (8) orifice diameters (8mm). This jet impingement array will be identified as F (5,8) where (5) refers to the chord wise spacing, and (8) to the span wise spacing and the letter (F) to the source of the heat transfer correlation used to describe the array by Florschuetz [14] and [15]. The remaining row is located at the leading edge. The trailing edge region consists of (0.6mm) wide slot which is (80mm) high, (in the spanwise direction). The cooling air mass flow rate is taken as  $28.7 \times 10^{-3}$  Kg/s, all of which passes through the insert and through the jet orifices to form the cooling jets but only half of it,  $14.35 \times 10^{-3}$  Kg/s, passes through the trailing edge slot

For the internal surfaces three distinct regions can be considered;

**(A) The Leading Edge Region**

Chupp *et al.*, [16], investigated the heat transfer at a simulated internal leading edge region of a turbine blade cooled by a single row of impinging air jets. The results of this experimental work consist of two heat transfer correlations. One for the jet stagnation region and one for the area around the jet stagnation region. These two correlations will be used here to characterize the heat transfer coefficients in this region. The mass flow rate through the leading edge row,  $\dot{m}_i$ , is taken as  $2.392 \times 10^{-3}$

Kg/s, which is one twelfth of the total coolant mass flow rate,  $\dot{m}_c$ . From Ref. [16] the spanwise averaged Nusselt Number for the jet stagnation region was correlated from the experimental results to be;

$$Nu_{stag} = 0.44 Re_j^{0.7} \left(\frac{d}{y_n}\right)^{0.8} \exp\left[-0.85\left(\frac{d_s}{d}\right)\left(\frac{d}{y_n}\right)\left(\frac{d}{d_{le}}\right)^{0.4}\right] \quad (29)$$

Where  $Re_j$  is the jet Reynolds number,  $d_{le}$  is the leading edge diameter and  $d_s$  is the distance between the insert and the leading edge blade wall, where  $Re_j = 13739, d = 1mm, d_{le} = 3.6mm, d_s = 2mm, y_n = 8mm$

Hence from equation (29);  $Nu_{stag} = 58, h_{stag} = 1825 W/m^2 K$

Around the stagnation region, Chupp et al, [16] established another correlation to found the averaged Nusselt Number from experimental results to be;

$$Nu_{asg} = 0.63 Re_j^{0.7} \left(\frac{d}{y_n}\right)^{0.5} \left(\frac{d}{d_{le}}\right)^{0.6} \exp\left[-1.27\left(\frac{d_s}{d}\right)\left(\frac{d}{y_n}\right)^{0.5} \left(\frac{d}{d_{le}}\right)^{1.2}\right] \quad (30)$$

From which it can be calculated;  $Nu_{asg} = 67, h_{asg} = 2121 W/m^2 K$

With the heat transfer coefficient determined for the leading edge region it only remains to specify the fluid temperatures in these areas ( $T_{stag}$ ) and ( $T_{asg}$ ) and these were both taken as (378K).

### B) The Pressure and Suction Surface Jet Arrays

The interior surface of the blade along the pressure and suction surfaces are cooled by (5) and (6) rows of jets respectively.

The heat transfer coefficients for the suction surface can be calculated using the correlation developed by Ref. [15]. The correlation is based on experimental results, the Nusselt Number resolved to one chordwise jet spacing is,

$$Nu_a = A_1 Re_j^m \left[1 - A_2 \left[\left(\frac{Z_n}{d}\right)\left(\frac{G_c}{G_j}\right)\right]^r\right] Pr^{0.333} \quad (31)$$

Where,  $A_1 = 0.67, A_2 = 0.237, m = 0.719$  and  $r = 0.317$

$$Re_j = \frac{G_j d}{\mu}$$

The calculated values of heat transfer coefficients are shown in table (1) in terms of the distance of jet spacing (x) along the blade surface.

Along the blade wall, (the impingement surface), the heat flux can be defined as:

$$q'' = h_a (T_s - T_{aw}) \quad (32)$$

Where ( $T_{aw}$ ) is the adiabatic wall temperature and can be defined in a non-dimensional effectiveness, ( $E_T$ ) as:

$$E_T = \frac{T_{aw} - T_j}{T_i - T_j} \quad (33)$$

Where,  $T_j$ : is the jet temperature,  $T_i$ : is the temperature of the initial cross flow,  $T_i > T_j$

The driving fluid temperature along the array ( $T_a$ ) can be taken as ( $T_{aw}$ ) hence once ( $E_T$ ) is known ( $T_a$ ) can be found. Florschuetz [14] estimates the values of ( $E_T$ ) for

an F(5,8) array and represented in table (1) together with the calculated values of ( $T_a$ ), where ( $T_j$ ) was taken as (378K) and ( $T_i$ ) as (477K).

For the pressure surface, the heat transfer coefficients are calculated according to equation (31) for which only  $Re_j$  and  $G_c/G_j$  will change and the results are listed in table (2). The value of ( $E_T$ ) reflects the influence of the higher temperature of the initial cross flow from the leading edge and because the ratio of the initial cross flow to the impingement jet array flow,  $M$ , has increased from 0.083 to 0.1, different ( $E_T$ ) values exist for the pressure surface. These values, together with the calculated values of ( $T_a$ ) based on a ( $T_i$ ) of (477K) and ( $T_j$ ) of (378K) as before, are shown in table (2).

Table (1) Result of Suction-Surface Heat Transfer Coefficients and Coolant Temperatures Obtained From Equations (31) and (33)

x(mm)	$h_a$ (W/m <sup>2</sup> K)	$E_T$	$T_a$ (K)
0 – 5	1581	0.258	403.5
5 – 10	1531	0.220	399.8
10 – 15	1514	0.198	397.6
15 – 20	1516	0.166	394.5
20 – 25	1540	0.120	389.9
25 – 30	1559	0.100	387.9

Table (2) Result of Pressure-Surface Heat Transfer Coefficients and Coolant Temperatures Obtained From Equations (31) and (33)

x(mm)	$h_a$ (W/m <sup>2</sup> K)	$E_T$	$T_a$ (K)
0 – 5	1601	0.278	405.5
5 – 10	1550	0.219	399.7
10 – 15	1533	0.182	396
15 – 20	1536	0.135	391.4
20 – 25	1552	0.106	388.5

**(c) The Trailing Edge Slot**

The average slot cooling air temperature is calculated according to the equation

$$T_{slot} = \frac{T_{sin} + T_{sout}}{2} \tag{34}$$

From Ref. [10], we found that,  $T_{sin} = 443k$ ,  $T_{sout} = 471k$

so from equation (34),  $T_{slot} = 458k$

From Ref. [17], the heat transfer coefficients were determined according to a correlation based on a turbulent flow between parallel plates:

$$Nu_{slot} = Nu_{fs} / (1 - C_T) \tag{35}$$

Where  $Nu_{fs}$ : is the nusselt number obtained from the fundamental solutions and  $C_T$ : is an influence coefficient.

From Rohsenow, et al [17] the values of  $Nu_{fs}$  and  $C_T$  are given for the distance along the slot. The result is shown in table (3) where (x) is the distance along the slot

Table (3) Results of Trailing Edge Slot Heat Transfer Coefficients Obtained from Equation (35).

x(mm)	$h_{slot}$ (W/m <sup>2</sup> K)
1	1651
1.5	1383
5	1249
15	1233

Analysis No. (2):

### Impingement Cooling Heat Transfer Correlations Based on Square Jet Array.

This analysis uses the same correlation as used in analysis (1), the only changes made are to the geometry, where the insert changed from a (5,8) array to a (5,5) array i.e.; the spanwise and chordwise spacing of the jet orifices were equal. This reduction in jet orifice spacing for all (12) rows results in an increase from (120) to (192) jet orifices i.e.; each row consists of (16) orifices in the span wise direction.

#### (A) The Leading Edge

The heat transfer coefficient is found to differ from that obtained in the previous analyses due changes in the span wise spacing of the jet orifices from (8) to (5), and therefore this value of heat transfer coefficient according to equation (29) is:

$$h_{stag} = 1773 W / m^2 K$$

Likewise, the heat transfer coefficient in the area around the stagnation region is calculated according to equation (30) to be:  $h_{asg} = 1834 W / m^2 K$

The coolant temperature in these regions,  $T_{stag}$  and  $T_{asg}$ , are again taken as (378K).

#### (B) The Pressure and Suction Surface Jet Arrays

The heat transfer coefficients are calculated according to equation (31) where due to the change in jet spacing, The parameters  $A_1, A_2, m$  and  $r$  now become;

$A_1 = 0.0919$ ,  $A_2 = 0.2636$ ,  $m = 0.7085$ ,  $r = 0.2393$ . The change in array geometry results in different values of effectiveness ( $E_T$ ) pertaining along the array. The values of ( $E_T$ ) are taken from Ref. [42]. The values of ( $T_a$ ) are calculated using equation (29) based on ( $T_j = 378 K$ ) and ( $T_i = 474 K$ ) The heat transfer coefficients and the values of ( $T_a$ ) along the pressure surface can be determined in the same procedure as for the suction surface. The results of this determination are shown in figure (11)

#### (c) The Trailing Edge Slot

The boundary conditions for the slot will be based on the turbulent flow between parallel plates as used in analysis (1).

#### Analysis No. (3):

#### Turbine Blade Cooling with Impingement and Film Cooling

In the previous analyses the impingement jets methods are used to cool the hot blade surfaces. These methods can, however be classified as internal methods of blade cooling, that is the cooling is achieved by the circulation of cooling air within the blade. The cooling requirements and stresses would be less severe if the heat transfer from the hot gas to the blade could be decreased by the process known as film cooling. Film cooling blades are not only cooled by convection, impingement methods, but they are also shielded from the outer hot gas with a film of spent cooling air ejected through the blade surface by rows of holes. The purpose of this analysis to determine the blade temperature distribution for such a film cooled blade. The cooling of the blade will consist of the same internal arrangement as utilized in analysis (1), that is an F(5,8) impingement jet array but in addition film cooling of the outer surface will be achieved through the use of (12) rows of (0.52 mm) diameter ejection holes distributed around the suction and pressure surfaces of the blade. Internally, the geometry remains unchanged from analysis (1). There are (120) jet orifices of (1mm) diameter whose jets impinge on the hot blade surfaces and which are arranged in (12) rows of (10) jets each, these are showed by Ref. [4] Over the suction and pressure surface jet arrays the jets

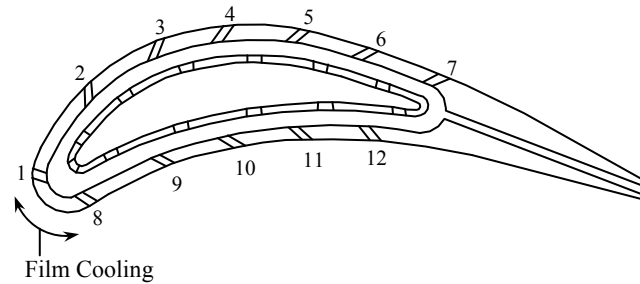


**Fig. (7) Blade Geometry**

are ordered with a spacing of (5) jet orifice diameters in the chord wise direction and (8) in the span wise direction. One half of the spent cooling air from these jets flows rearwards towards the trailing edge and exits the blade through the trailing slot as in analysis (1). The remaining spent cooling air exits the blade through a series of film cooling ejection holes distributed throughout the blade wall. There are in total (468) film cooling holes of (0.52mm) diameter. These are arranged in (12) rows each containing (39) holes each. (7) of the rows are spaced along the suction surface while (5) are spaced along the pressure surface. Within each row the holes are spaced a distance of (2mm) apart. The film cooling holes consist of two rows with an ejection angle of  $64^{\circ}$ , rows 1 and 8 and 10 rows with an ejection angle of  $45^{\circ}$ .

#### Specification of Boundary Conditions

The specification of the boundary conditions can be sub-divided into two main areas:

1-The internal boundary conditions, which will be dealt with in a similar manner to that used in analysis (1), as the internal cooling arrangement and geometry remains unaltered from this analysis.

2-The external boundary conditions, which must take into account the presence of the ejected cooler film of air over the outer surface of the blade.

#### Internal Boundary Conditions

The boundary conditions at the leading edge are unaltered from analysis (1), Likewise the heat transfer coefficients for the suction and pressure surfaces jet arrays also remain unchanged

However the value of  $T_a$ , the array driving temperature does change because the temperature of the initial cross flow,  $T_i$  is reduced due to the effect of film cooling in reducing the heat transfer to the blade. The trailing edge slot conditions also change because the temperature of the cooling air entering the slot,  $T_{sin}$  is reduced again because of the decrease in heat transfer to the blade.

#### Suction Surface-Coolant Temperatures

The value of  $T_i$ , from a series of preliminary runs was determined to be (465K) which is less than the value obtained in analysis (1) due to the protection obtained from the film cooling which reduces the heat transfer to the blade and consequently to the cooling air.

This value of  $T_i$  is then used in equation (33) to obtain the values of ( $T_a$ ) as shown in figure(13) where ( $E_T$ ) is obtained from analysis (1)

#### Pressure Surface – Coolant Temperatures

Again the initial cross flow temperature,  $T_i$  is reduced to (465 K) and using the same values of  $E_T$  as for analysis (1),  $T_a$  is determined and the results shown in figure(13)

#### The Trailing Edge Slot

The reduction in the heat addition to the cooling air along the jet arrays at the leading edge due to the film cooling reduces the temperature of the coolant entering the slot and hence alters the slot boundary conditions. The boundary conditions are based on the parallel plate flow with the following required parameters;  $T_{sin} = 423 K$ ,  $T_{sout} = 428 K$ ,  $T_{slot} = 425.5 K$

The calculated values of  $h_{slot}$  along the slot are presented in table (4)

Table (4) Results of Trailing Edge Slot- Heat Transfer Coefficients Obtained from Equation (35)

x(mm)	$h_{slot}(W/m^2K)$
1	1673
1.5	1404
5	1282
15	1265

#### External Boundary Conditions

The ejection of cooling air through the film cooling holes results in a change in the conditions existing along the outer profile of the blade. This section seeks to specify the new boundary conditions that now exist as a result of the film cooling used on this blade.

An analysis of the boundary layer with film cooling results in the specification of the heat flux to the blade surface from the hot gas as;

$$q'' = h_{ext}(T_{aw} - T_s) \quad (36)$$

Where  $q''$  is the heat flux to the blade.

$h_{ext}$  is the heat transfer coefficient without film cooling, i.e.; as given by Figure (3).

$T_s$  the blade wall surface temperature,  $T_{aw}$  is the adiabatic wall temperature.

The adiabatic wall temperature can be non-dimensionalized as a film cooling effectiveness,  $E_f$  defined by;

$$E_f = \frac{T_g - T_{aw}}{T_g - T_{c2}} \quad (37)$$

Where  $T_g$  is the gas temperature.

$T_{c2}$  is the temperature of the coolant leaving the film cooling holes, as shown in Figure (8).

the effectiveness ( $E_f$ ) is defined for the  $45^\circ$  and  $64^\circ$  ejection angles as :

$$E_{f_{45}} = 0.3901 / (1 + 0.44 R^{0.8}) \quad (38)$$

$$E_{f_{64}} = 0.3901 / (1 + 0.46 R^{0.8}) \quad (39)$$

Where,

$$R = \left( \frac{x}{1.2 Se} \right) \left[ \text{Re}_{c2} \left( \frac{\mu_{c2}}{\mu_g} \right) \right]^{-0.25} \quad (40)$$

$Se = 0.4084 \text{ mm}$ ,  $\mu_{c2} = 23.8 \times 10^{-6} \text{ kg/m.s}$ ,  $\mu_g = 40.8 \times 10^{-6} \text{ kg/m.s}$ ,  $\text{Re}_{c2} = 3207$

The value of  $T_g$  used in equation (37) varies from row to row because the films from successive rows reinforce each other, i.e.; the film temperature upstream of a row becomes the gas temperature of the next downstream row. Rows (1) and (8), which are the first rows on the suction and pressure surfaces inject the coolant into the external flow which has a temperature of 963K the second rows, i.e.; (2) and (9), inject their coolant into the film provided by rows (1) and (8) which is now at a lower temperature. This reduction in the effective  $T_g$  continues for the other downstream rows also. The effective  $T_g$  used for each row is shown in table (5). This temperature is equal to the value of  $T_{c \text{ film}}$  existing just upstream of the row. For example row (2) is 7.7 mm downstream of row (1). For  $x=7.7 \text{ mm}$ ,  $E_{f64}$  can be calculated to be 0.2028 from which  $T_{c \text{ film}}$  is 853.5 K, based on a  $T_g$  of 963 K. This value of  $T_{c \text{ film}}$  is now used as the effective gas temperature,  $T_g$  for the calculations for the second row.

Table (5) Results of Effective Gas Temperature  
Obtained from Equation (37)

Film Cooling Row	Effective $T_g$ (K)
1	963
2	853.5
3	752
4	669
5	609
6	564
7	529
8	963
9	847
10	742
11	663
12	603

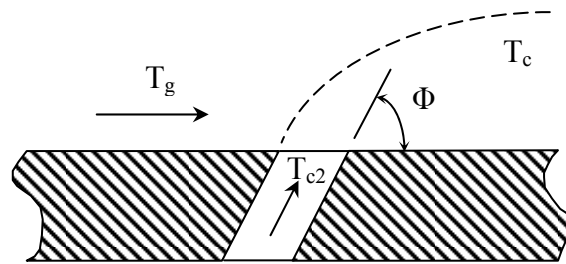


Fig. (8) Film Cooling Hole

## RESULTS AND DISCUSSIONS

Prediction of blade temperature distribution was performed by using three cases, hence three different heat transfer correlation were used.

In the three cases, the blade cooling was assumed to be by using a blade with impingement cooling and trailing edge ejection. The reason behind this choice is that this type of cooling has a wide range of use in practice.

### Analysis No. (1):

The internal boundary conditions for analysis (1) can be summarized in Figure (9), showing the values of the heat transfer coefficient and the fluid temperature associated with each region of the blade.

The temperature contour pattern of Figure (10) shows the maximum temperature of (662 K) at the leading edge region with falling temperatures along both the pressure and suction surfaces followed by a rise in temperature towards the trailing edge. Closer inspection of figure (10) shows that over the pressure surface, from the leading edge, the temperature falls quite rapidly before leveling out and then increasing continuously

towards the trailing edge. However along the suction surface the fall in temperature from the leading edge region is not great, but this reduction extends over a greater length of the blade than that on the pressure surface. However the minimum temperature on the suction surface is approximately (20 K) higher than the minimum temperature on the pressure surface i.e., over the mid-chord regions of the blade, the suction surface is hotter than the pressure surface. At the trailing edge the situation is reversed with the pressure surface hotter than the suction surface.

These differences in temperatures between the two surfaces can be accounted for by a number of factors:

- 1) The blade structure is hollow which reduces the connectivity between the pressure and suction surfaces and hence reduces the tendency to smooth out temperature differences between the two areas.
- 2) As a result of (1) above, the influence of the variation of external heat transfer coefficient is much greater. For example, 8mm along the suction surface (8,S.S.), there is a rapid fall in  $h_{ext}$  which results the reduction in temperature along the suction surface at (8,S.S.). After this point as  $h_{ext}$  begins to fall again the temperature levels also fall. Comparing this to the pressure surface where  $h_{ext}$  falls very quickly from the stagnation point to (5,P.S.), before rising slowly. The temperature variation is seen to mimic this by falling continuously to (5,P.S.). The mid-chord regions also exhibit the effect of  $h_{ext}$ , with the decreasing temperature along the suction surface from (10,S.S.) to (35,S.S.) reflecting the decreasing  $h_{ext}$  while the rise in temperatures along the pressure surface from (18,P.S.) to (28,P.S.) mimicing the rising  $h_{ext}$ .
- 3) The cooler pressure surface can also be accounted for by the higher values of the impingement heat transfer coefficients in this region. The variation of the array heat transfer coefficients does affect the variation of the resulting temperature distribution but because these array variations are much smaller than the variation of  $h_{ext}$  their influence on the temperature variations is consequentially less.
- 4) The trailing edge temperature distribution is more complex than the other blade regions and reflects both the variations of  $h_{ext}$  as well as the varying blade wall thickness around the trailing edge slot. The general increase in temperature towards the trailing edge can also be accounted for by the lower value of  $h_{slot}$  when compared to the impingement values,  $h_a$ .

#### Analysis No. (2):

The internal boundary conditions for this analysis are presented in Figure (11), While the external boundary conditions are the same as in analysis (1)

The results of the thermal analysis are presented in Figure (12) shows a pattern very similar to the analysis (1), (5,8) array with maximum temperature of (688 K) at the leading edge. The temperature levels fall over the mid-chord regions before rising towards the trailing edge. For the purpose of comparing the (5,8) and (5,5) arrays, It is clear that while the pattern remains very similar, the (5,8) case, with less jet orifices produces lower blade temperatures than the (5,5) case which has more jet orifices. This apparent contradiction occurs due to the reduction in  $Re_j$  as the number of orifice increase leading to a reduction in the levels of the heat transfer coefficient. For the trailing edge region of the blade, the difference between the blade surface temperatures is very small reflecting the diminishing influence of changes to the cooling arrangement of the insert and also reflecting the similarity of the boundary conditions along the trailing edge slot.

Analysis No. (3):

Figure (13) shows the internal boundary conditions of analysis (3) when the blade is cooled with film cooling. Figure (14) illustrates the temperature contour pattern within the blade and shows the significant effect that film cooling has on the blade temperatures. Again the highest temperatures occur at the leading edge corresponding to the area of highest ( $h_{ext}$ ) and no film cooling. Across the pressure and suction surfaces the temperatures fall considerably due to the effect of the multiple rows of film cooling and low temperature reach to (430 K).

Due to the lack of the film cooling around the leading edge, the blade temperatures in this region remain nearly high for this analysis, with the film cooling as for analysis (1), without the film cooling. However it is clear that the blade temperature decreases rapidly after this area and results in the film cooled blade as much as (170 K) cooler than the blade without film cooling. The rise in temperature at the trailing edge can be accounted for by a number of factors such as the reducing trailing edge slot heat transfer coefficient together with the reducing value of ( $E_f$ ) over this region as the last row of film cooling holes is located well upstream of this area.

Figure (15) shows comparison between blade surface temperature for the three methods of analyses used in this work and with that obtained in using the finite element method, Ref [4]. It is clear seen that in all analyses the maximum temperature occurs at the leading edge. In the pressure and suction surfaces the temperature decreases followed by a rise in temperature toward the trailing edge.

It is obvious from figure (15) that analysis (3) with the film cooling gives lower temperature distribution than the other analyses. For the remaining analyses without the film cooling, it can be seen that analysis (1) for (5,8) array and trailing edge heat transfer based on plate flow and lower than analysis (2) which has more jet array for the insert geometry i.e.,(5,5) array and trailing edge heat transfer based on plate flow and this figure shows a great similarity between the finite difference and the finite element results, which seems to coincide in most regions along blade surface. The differences between the results of the two methods are due to the differences in the technique of each method as well as the use of transformation theory, which depends on the transformation of curved boundaries of blade profiles into straight lines.

An inspection to the graphs, it can be seen that the difference of the finite difference results from the finite element method is very small. This difference was calculated to be (3.503 %) as maximum value and it falls to (0%) in most regions.

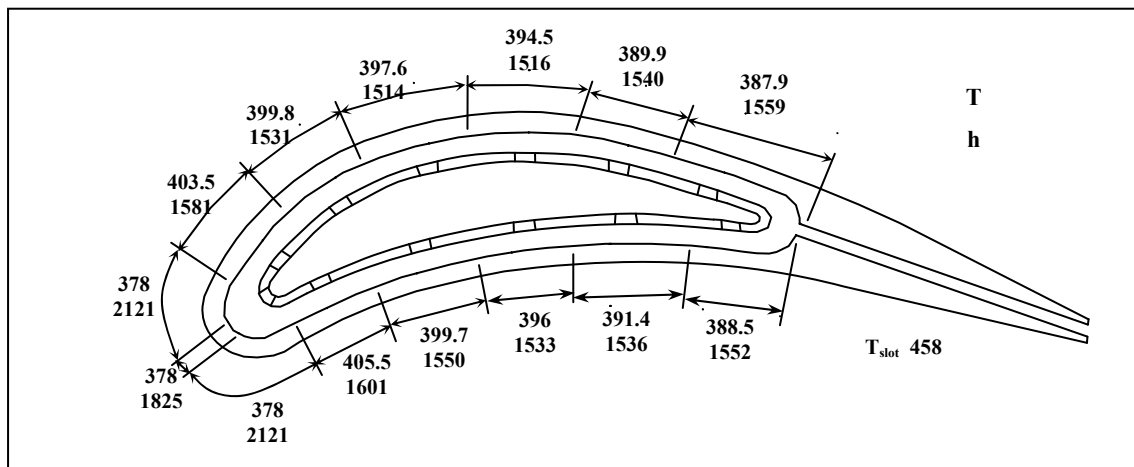


**Figure (9) Internal Boundary Condition-Analysis (1)**

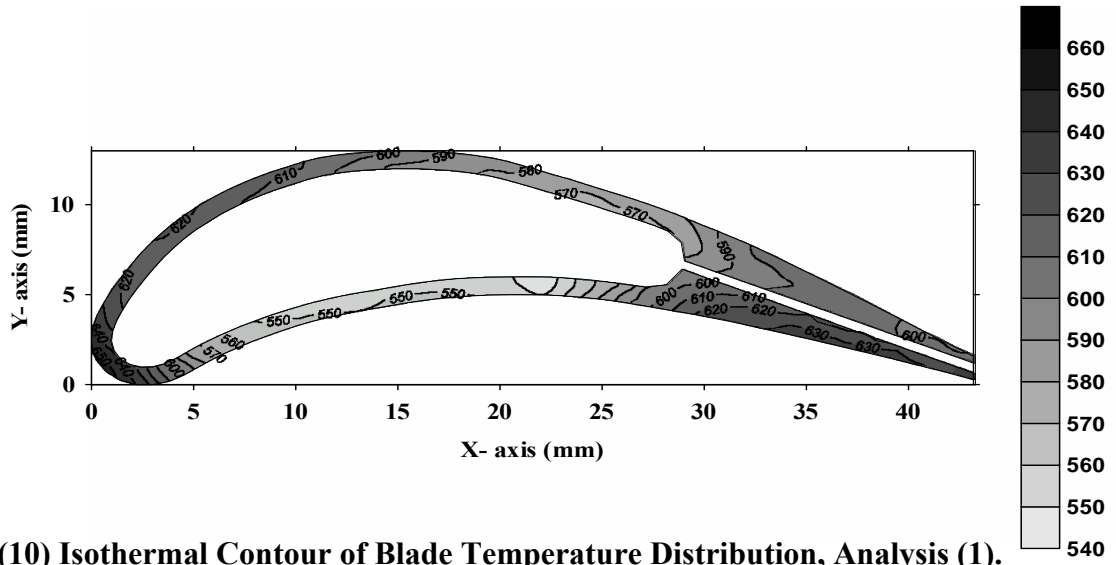


Figure (10) Isothermal Contour of Blade Temperature Distribution, Analysis (1).

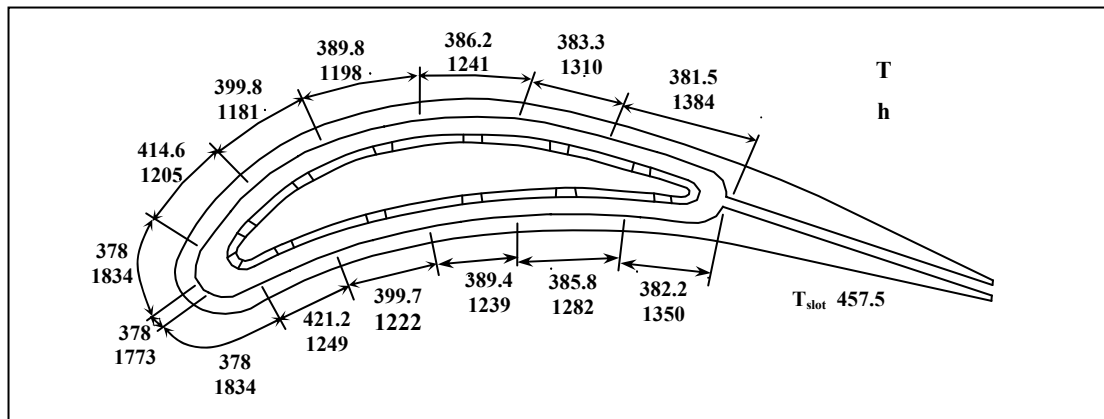


Figure (11) Internal Boundary Condition-Analysis (2)

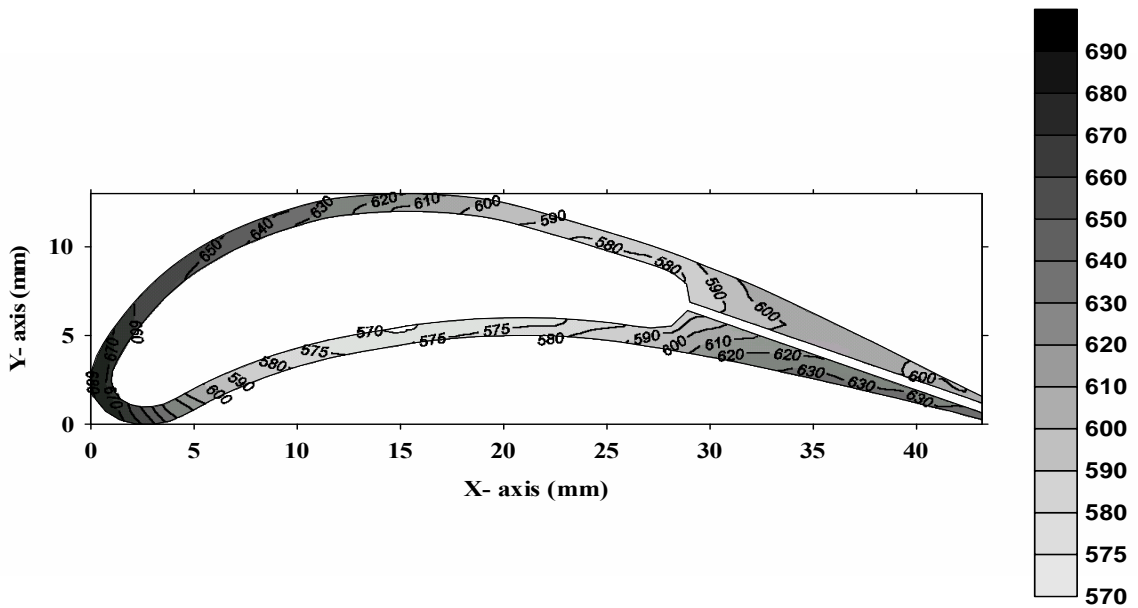


Figure (12) Isothermal Contour of Blade Temperature Distribution, Analysis (2).

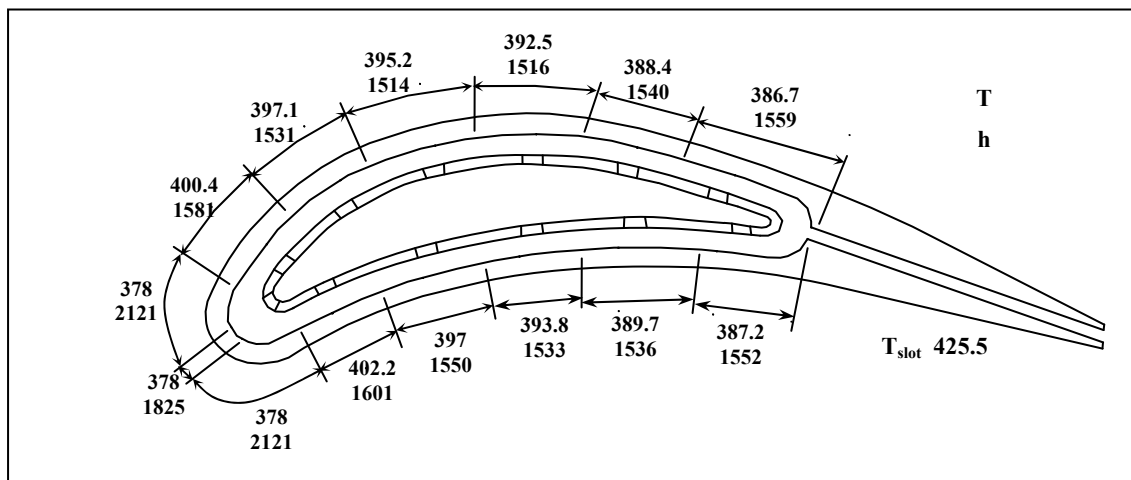


Figure (13) Internal Boundary Condition-Analysis (3)

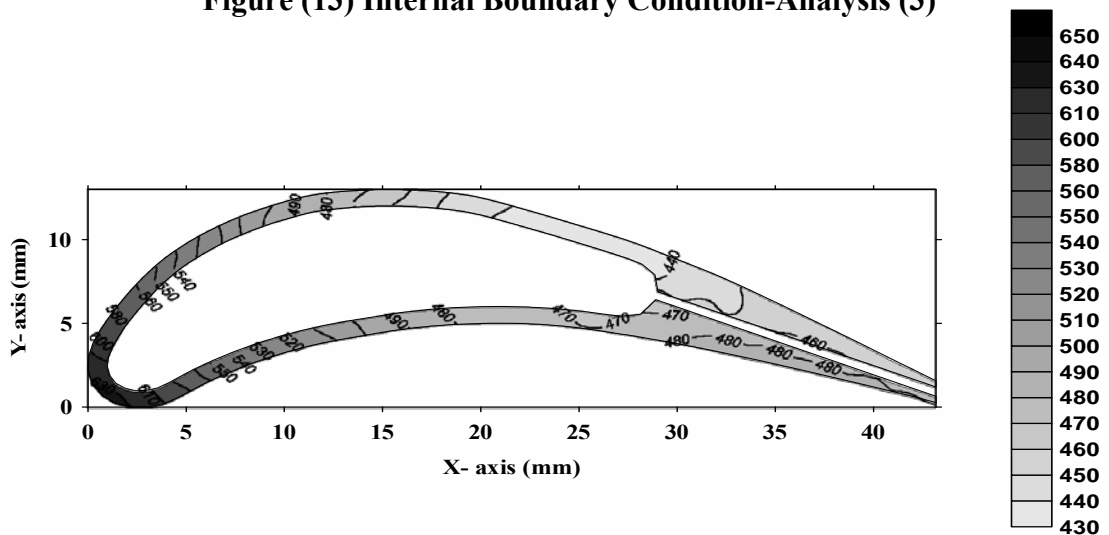


Figure (14) Isothermal Contour of Blade Temperature Distribution, Analysis (3)

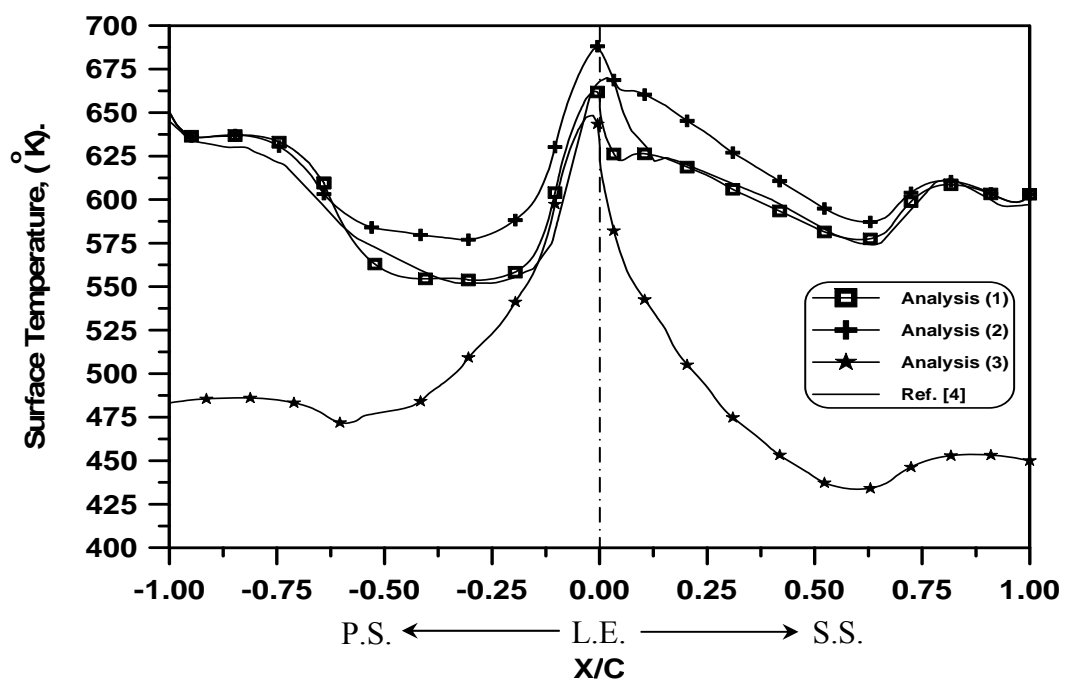


Figure (15) Comparison between Blade Surface Temperature For the Three Analyses and Ref.[4]

## CONCLUSIONS

The main conclusions that can be drawn from this work are summarized in the following points:

1- Three case studies are used for thermal analyses of the blade, which requires the specification of external and internal boundary conditions. It is also found from the results obtained that the best cooling method to the turbine blade have been obtained for the third case when the blade cooled by impingement and film cooling method.

2- The analysis procedure used gave a good results in terms of their accuracy when compared with the results of other researchers.

3- Numerical finite difference was used successfully in obtaining temperature distribution for complicated geometries as compared to the finite element results.

4- The body fitted coordinates method represents an efficient flexible tool for treating difficult geometries.

5- An impingement-cooled blade can be dealt with a two-dimensional thermal analysis through the use of heat transfer correlations, which provide spanwise averaged values of the heat transfer coefficients.

6- The effect of increasing the number of cooling air jets, which impinge on the hot blade surfaces, results in an increase in the blade temperature. This is because the increase in number of jets of high intensity cooling regions is accompanied by a reduction in the jet Reynolds number.

7- Several different heat transfer correlations can be used to describe the impingement jet array areas as they all produce similar values of heat transfer coefficients and hence similar blade temperatures.

8- Film cooling can be analyzed by varying the external boundary conditions of the blade and results in an appreciable reduction in blade temperatures about (170 K) cooler than the blade without film cooling.

## REFERENCES

- [1] El-Wakil, M.M., "Power-Plant Technology", McGraw-Hill, Inc., 1985.
- [2] Turner A.B., Long C.A., Childs P.R. N., Hills N.J., and Millward J.A., "A Review of Some Current Problems in Gas Turbine Systems", [http:\ www.google.com](http://www.google.com), (Key Words "Gas Turbine"), 1998.[Paper]
- [3] Jack D. Mattingly, "Elements of Gas Turbine Propulsion" McGraw-Hill, Inc., 1996.
- [4] Walker M.J.B., "Turbine Blade Internal Heat Transfer", M.Sc. Thesis, Cranfield Institute of Technology, 1989.
- [5] Jaleel J. M., "The Effectiveness of Finite Difference method on Curved Boundary AirCooled Turbine Blades", Journal of Military College of Engineering, No.25, pp. 19-32, 2001.
- [6] Kudor D.S., "Effect of Cooling Air Passage Shape on Gas Turbine Blade Temperature Distribution", M.Sc. Thesis Al-Mustansiria University, Iraq, 2003.
- [7] Marie L.H., Eriksson L.E. and Suden B., "Convective Heat Transfer on an Inlet Guide Vane", [http:\ www.google.com](http://www.google.com), (Key Words "Turbine Blade Cooling"), 2003.[Paper]

- [8] Ken I.T. and Takasago S.A., “Contribution of Heat Transfer to Turbine Blades and Vanes for High Temperature Industrial Gas Turbines”, [http:\ www.google.com](http://www.google.com), (Key Words “Turbine Blade Cooling”), 2000.[Paper]
- [9] Stefan L.F., “Surface Temperature Mapping of Gas Turbine Blading by Means of High Resolution Pyrometry”, [http:\ www.google.com](http://www.google.com), (Key Words “Turbine Blade Cooling”), 2001.[Paper]
- [10] Thompson J.F., “Grid Generation techniques in Computational Fluid Dynamics”, AIAA Journal, Vol.22, No.11, November, pp. 1505-1522, 1984.
- [11] Hoffmann K.A., “Computational Fluid Dynamics for Engineers”, 1989.
- [12] Anderson J.D., “Computational Fluid Dynamics”, McGraw-Hill, Inc., 1995.
- [13] Anderson D.A., John C. Tennehill and Richard H. Pletcher, “Computational Fluid Mechanics and heat Transfer”, McGraw-Hill Company, 1984.
- [14] Florshuetz L.W. Metzger D.E., Su C.C., Isoda Y. and Tseng H.H., “Jet Array Impingement Flow Distribution and Heat Transfer Characteristics-Effect of Initial Crossflow and Nonuniform Array Geometry”, NASA CR 3630, 1982.
- [15] Florshuetz L.W. Metzger D.E. and Truman C.R., “Jet Impingement with Crossflow-Correlation of Streamwise Resolved Flow and Heat Transfer Distributions”, NASA CR 3373, 1981.
- [16] Chupp R.E., Helms H.E., McFadden P.W. and Brown T., “Evaluation of Internal Heat Transfer Coefficients for Impingement- Cooled Turbine Airfoils”, Journal of Aircraft, Vol.6, PP 203-208, 1969.
- [17] Rohsenow W.M., Hartnet J.P. and Ganic E.N., “Handbook of Heat Transfer Fundamentals”, 2<sup>nd</sup> ed. McGraw-Hill Book Co., 1987

NOMENCLATURE

Symbol	Description	Unit
$A_1, A_2$	Correlating Parameters in Equation (31)	–
$d$	Jet Orifice Diameter	mm
$E_f$	Film Cooling Effectiveness	–
$G_j$	Jet Mass Velocity for One Jet Row	kg/m <sup>2</sup> .s
$h_{ex}$	External Heat Transfer Coefficient	W/m <sup>2</sup> . K
$h_{in}$	Internal Heat Transfer Coefficient	W/m <sup>2</sup> . K
$h_{slot}$	Heat Transfer Coefficient of the Slot	W/m <sup>2</sup> . K
$i, j$	The Indexes Increases Along the x and y Axes	–
$J$	Jacobian Transformation	–
$k$	Thermal Conductivity	W/m. K

$Nu$	Nusselt Number	–
$P$	Source Term in Poisson's Equation is Used to Attract $\xi$ -Coordinate lines	–
$Pr$	Prandtl Number	–
$q''$	Heat Flux	W/m <sup>2</sup>
$Q$	Source Term in Poisson's Equation is Used to Attract $\eta$ -Coordinate lines	–
$R$	Correlating Parameter in Equation (41)	–
$S, S_\xi, S_\eta$	Distance Along Blade Surface	mm
$T$	Temperature	K
$T_{aw}$	Adiabatic Wall Temperature	K
$T_\infty$	Fluid (Air) Temperature	K
$x$	Physical Coordinates	mm
$x_n$	Chordwise Spacing	mm
$y$	Physical Coordinates	mm
$y_n$	Spanwise Spacing	mm
$Z_n$	Insert to Blade Wall Distance	mm

Greek Symbol

$\Delta\xi, \Delta\eta$	Spatial Steps in Computational Domain	–
$\phi$	Ejection Angle	Deg.

Abbreviations

P.S.	Pressure Surface
S.S.	Suction Surface